UCLA
COMPUTATIONAL AND APPLIED MATHEMATICS

Oscillatory Instability of Traveling Waves for a KdV-Burgers Equation

Robert L. Pego
Peter Smereka
Michael I. Weinstein

August 1992

CAM Report 92-38

Department of Mathematics
University of California, Los Angeles
Los Angeles, CA. 90024-1555

Oscillatory instability of traveling waves for a KdV-Burgers equation

Robert L. Pego, [1] Peter Smereka, [2] and Michael I. Weinstein [3]

August 4, 1992

Abstract

The stability of traveling wave solutions of a generalization of the KdV-Burgers equation:

$$\partial_t u + u^p \partial_x u + \partial_x^3 u = \alpha \partial_x^2 u \ , \tag{1.1}$$

is studied numerically as the parameters p and α are varied. The eigenvalue problem for the linearized evolution of perturbations is analyzed by numerically computing Evans' function, $D(\lambda)$, an analytic function whose zeros correspond to discrete eigenvalues. In particular, the number of unstable eigenvalues in the complex plane is evaluated by computing the winding number of $D(\lambda)$. We find evidence that a Hopf bifurcation occurs for oscillatory traveling wave profiles in certain parameter ranges. Dynamic simulations suggest that the bifurcation is *subcritical*: No stable time periodic solution is found.

AMS (MOS) Subject Classifications: 35Q20, 35P15, 34B25, 65L15

Key Words: shock profile, Hopf bifurcation, Evans function, undular bore

---

[1] Department of Mathematics & Institute for Physical Science and Technology, University of Maryland. Supported by NSF Grant DMS DMS-9196155.

[2] Department of Mathematics, University of California at Los Angeles. Supported by a National Science Foundation Postdoctoral Fellowship.

[3] Department of Mathematics, University of Michigan, Ann Arbor. Supported by NSF Grant DMS-9201717.

1. Introduction

We consider the generalized KdV-Burgers equation

$$\partial_t u + u^p \partial_x u + \partial_x^3 u = \alpha \partial_x^2 u \ , \tag{1.1}$$

a model for long wave propagation in nonlinear media with dispersion and dissipation. Here $p \geq 1$ and $\alpha > 0$. The case $p = 1$ is known as the KdV-Burgers equation . Its traveling waves model the propagation of undular bores in shallow water [24]. For $\alpha = 0$, equation (1.1), now a generalized KdV equation, has solitary wave solutions $u(x,t) = \phi_0(x - ct)$ for any $c > 0$, whose profile $\phi_0(\xi)$ satisfies

$$-c\phi_0 + \frac{1}{p+1}\phi_0^{p+1} + \partial_\xi^2 \phi_0 = 0 \ , \quad \phi_0(\xi) \to 0 \quad \text{as } \xi \to \pm\infty \ . \tag{1.3}$$

Explicitly,

$$\phi_0(\xi) = \beta \, \mathrm{sech}^{2/p} \gamma\xi \quad , \quad \text{where} \quad \beta = (\tfrac{1}{2}c(p+1)(p+2))^{1/p} \ , \ \gamma = \tfrac{1}{2}p\sqrt{c} \ .$$

This wave is known to undergo a transition from stability ($p < 4$) to instability ($p > 4$) as the parameter p passes through the critical value $p_c = 4$, cf. [2,3,5,13,17,21-23].

For $\alpha > 0$, equation (1.1) has a family of traveling wave solutions, whose properties are summarized as follows (cf. [4,17]).

Theorem 1.1 *Given $\alpha > 0$ and $c > 0$, equation (1.1) has a solution $u(x,t) = \phi(x - ct)$, unique up to translation, with wave profile $\phi(\xi)$ satisfying*

$$-c\phi + \frac{1}{p+1}\phi^{p+1} + \partial_\xi^2 \phi = \alpha \partial_\xi \phi \ , \quad \xi \in \mathbb{R} \ , \tag{1.4}$$

$$\phi(\xi) \to \begin{cases} u_L & \text{as } \xi \to -\infty \ , \\ 0 & \text{as } \xi \to \infty \ . \end{cases} \tag{1.5}$$

Here, $u_L = (c(p+1))^{1/p}$ is the unique positive solution of $-cu_L + u_L^{p+1}/(p+1) = 0$. If $\alpha > 2\sqrt{pc}$, the profile ϕ is monotonically decreasing , while if $\alpha < 2\sqrt{pc}$, then $\phi(\xi) \to u_L$ in an oscillatory fashion as $\xi \to -\infty$. As $\xi \to +\infty$, the profile satisfies

$$\phi(\xi) \sim e^{\nu(\xi - \xi_0)} \ , \qquad \partial_\xi \phi(\xi) \sim \nu e^{\nu(\xi - \xi_0)} \ , \tag{1.6}$$

for some ξ_0, *where* $\nu = \frac{1}{2}(\alpha - \sqrt{\alpha^2 + 4c}) < 0$.

In the $\phi - \phi'$ phase plane, the wave profile corresponds to the unique trajectory that connects the unstable critical point $(u_L, 0)$ to the saddle point $(0, 0)$. See figure 1.

INSERT near here

Figure 1. (a) $\phi - \phi'$ phase plane, (b) $\phi(\xi)$ vs ξ.

As $\alpha \to 0$ for fixed c, p (and ξ_0), the wave profile converges in a very nonuniform fashion. At $\alpha = 0$, the stable manifold of the saddle point $(0, 0)$ is a homoclinic loop given by the level curve $E = 0$ of the conserved quantity

$$E(\phi, \phi') = \frac{1}{2}\phi'^2 - \frac{1}{2}c\phi^2 + \frac{1}{(p+1)(p+2)}\phi^{p+2}. \tag{1.7}$$

Level curves for $E < 0$ correspond to closed periodic orbits lying inside the homoclinic loop and encircling a center at $(u_L, 0)$.

As α becomes positive, the homoclinic loop breaks, and because $dE/d\xi = \alpha\phi'^2 \geq 0$, the stable manifold is trapped in the region $E < 0$, approaching the unstable spiral point $(u_L, 0)$, and fills the region $E < 0$ ever more densely as $\alpha \to 0$. As $\alpha \to 0$, the wave profile $\phi(\xi)$ converges uniformly to the solitary wave profile $\phi_0(\xi)$ for $\xi \geq x_0$, for any fixed x_0 (assuming ξ_0 is chosen appropriately). But globally in ξ, the profile $\phi(\xi)$ has a long oscillatory *tail*, which tapers exponentially to u_L as $\xi \to -\infty$.

When $\alpha > 2\sqrt{pc}$ and the wave profile $\phi(\xi)$ is monotone, the traveling wave $\phi(x - ct)$ is known to be stable [16,17]. Stability persists for "mildly oscillatory" waves with α near $2\sqrt{pc}$, cf. [12]. Since for $p > 4$ and $\alpha = 0$ the solitary wave $\phi_0(x - ct)$ is unstable, a transition to instability is expected to occur as $\alpha \to 0$ for any fixed $p > 4$. The results of [17] suggested that this transition might occur via a complex pair of eigenvalues crossing the imaginary axis. In the present paper, we present numerical evidence that this is indeed the case, and that when $p > 4$ and α is decreased, the traveling wave loses stability in a subcritical Hopf bifurcation.

2. Linear stability

In order to consider the linear stability of the traveling wave, we seek solutions of (1.1) in the form

$$u(x,t) = \phi(x-ct) + v(x-ct,t)$$

and neglect terms which are $\mathcal{O}(v^2)$. The linear evolution equation for the perturbation $v(\xi,t)$ is

$$\partial_t v = \mathcal{A}v \ , \quad \mathcal{A} = \partial_\xi(-\partial_\xi^2 + \alpha\partial_\xi + c - \phi(\xi)^p) \ , \tag{2.1}$$

where $\xi = x - ct$. We intend to study transition to instability by examining the spectrum of $\mathcal{A}$ as the parameters α, c and p are varied. We consider $\mathcal{A}$ as an operator on $L^2(\mathbb{R})$ with domain $D(\mathcal{A}) = H^3(\mathbb{R})$, the Sobolev space of functions with L^2 derviatives up to third order. Regarding the structure of the spectrum, we refer to Henry [9, Chapter 5]. The spectrum is the same in $L^p(\mathbb{R})$, $1 \le p < \infty$, or in the space of bounded uniformly continuous functions on $\mathbb{R}$. The spectrum consists of *discrete spectrum* (isolated eigenvalues of finite multiplicity) and *essential spectrum* (everything else not in the resolvent set). Since $\phi(\xi)$ approaches constant limits 0 and u_L at an exponential rate as $\xi \to \pm\infty$ respectively, the essential spectrum is determined from that of the constant coefficient operators

$$\mathcal{A}_+ = \partial_\xi(-\partial_\xi^2 + \alpha\partial_\xi + c) \ , \tag{2.2}$$

$$\mathcal{A}_- = \partial_\xi(-\partial_\xi^2 + \alpha\partial_\xi + c - u_L^p) \ . \tag{2.3}$$

Let $S_e^\pm$ denote the spectrum of $\mathcal{A}_\pm$. Using the Fourier transform, one finds that (since $u_L^p - c = pc$)

$$S_e^+ = \{\lambda : \lambda = -\alpha\tau^2 + i\tau(\tau^2 + c), \tau \in \mathbb{R}\} \ , \tag{2.4}$$

$$S_e^- = \{\lambda : \lambda = -\alpha\tau^2 + i\tau(\tau^2 - pc), \tau \in \mathbb{R}\} \ . \tag{2.5}$$

The sets S_e^+ and S_e^- are two curves in the closed left half plane. The complement of $S_e^+ \cup S_e^-$ consists of a number of disjoint connected components. Let Ω^+ denote the component which contains the right half plane. Then the essential spectrum can be characterized by the following result which is proved in [17].

Proposition 2.1 *Let $\alpha > 0$. The essential spectrum of $\mathcal{A}$ contains $S_e^+ \cup S_e^-$, but contains no point of the component Ω_+. In particular, points in the spectrum of $\mathcal{A}$, lying in Ω_+, must be isolated eigenvalues.*

The situation is simpler for the case $\alpha = 0$, when $\phi(\xi)$ is replaced by $\phi_0(\xi)$, which tends to 0 as $\xi \to \pm\infty$. Let $\mathcal{A}_0 = \partial_\xi(-\partial_\xi^2 + c - \phi_0(\xi)^p)$. In this case the essential spectrum is $S_e^0 = \{\lambda : \lambda = i\tau(\tau^2 + c), \tau \in \mathbb{R}\}$, which is the imaginary axis.

Regarding the discrete spectrum of $\mathcal{A}_0$, it has been shown in [17, Theorem 3.4] that: For $p < 4$, $\mathcal{A}_0$ has no discrete eigenvalues λ with $Re\,\lambda \neq 0$. For $p > 4$, $\mathcal{A}_0$ has a pair of symmetrically placed eigenvalues $\pm\lambda_0(p) \in \mathbb{R}$, $\lambda_0 > 0$. Each of these eigenvalues is simple, having multiplicity one. There are no other isolated eigenvalues λ with $Re\,\lambda \neq 0$. However, $\lambda = 0$ is an eigenvalue embedded in the essential spectrum of $\mathcal{A}_0$, with eigenfunction $\partial_\xi\phi_0(\xi)$, associated with the translation invariance of (1.1). See figure 2.

INSERT near here

Figure 2. Spectrum of $\mathcal{A}_0$ for (a) $p < 4$ and (b) $p > 4$.

As $p \downarrow 4$, the eigenvalue $\lambda_0(p) \to 0$, merging with the origin at the transition value $p = 4$. Now when $\alpha > 0$, $\lambda = 0$ is an eigenvalue of $\mathcal{A}$ embedded in the essential spectrum, with eigenfunction $\partial_\xi\phi(\xi)$. From the considerations of section 1, we expect that for any $p > 4$ and c fixed, as $\alpha \to 0$ a transition to linear instability should occur via the appearance of one or more eigenvalues of $\mathcal{A}$ in the right half plane. However, in [17] it was proved that the mechanism for transition to instability cannot be like that in the case $\alpha = 0$: No eigenvalue may merge with the origin while α remains strictly positive.

In this paper we show numerically, that a transition to instability does occur via a pair of complex conjugate eigenvalues crossing from the left half plane to the right half plane, as α decreases. There is additional evidence that more pairs of eigenvalues cross into the right half plane as α is decreased further. In figure 3 we display some of the results of our numerical computations for $p = 6$, $c = 1$, and (a) $\alpha = .08$, (b) $\alpha = .07$. The solid curves correspond to the curves S_e^+ and S_e^-, which bound the essential spectrum of $\mathcal{A}$. (From (2.4)-(2.5) it is seen that S_e^+ and S_e^- approach the imaginary axis as α decreases toward zero.) In Figure 3(b) the crosses indicate isolated eigenvalues at $\lambda = .0667 \pm 1.985i$,

for $\alpha = .07$. These eigenvalues are zeros of Evans' function $D(\lambda)$, to be described below. In Figure 3(a) the crosses indicate the corresponding zeros of $D(\lambda)$ for $\alpha = .08$. As α decreases, these zeros move to the right, crossing first the curve S_e^- to become isolated eigenvalues in Ω_+, then crossing the imaginary axis, indicating a transition to instability.

INSERT near here

Figure 3. Spectrum of $\mathcal{A}$ for (a) $\alpha = .08$, (b) $\alpha = .07$.

3. Evans' function and eigenvalues

The approach we use to determine the isolated eigenvalues of the operator $\mathcal{A}$ in (2.1) is based on the numerical computation of Evans' function $D(\lambda)$, an analytic function whose zeros correspond to these isolated eigenvalues. J.W. Evans introduced $D(\lambda)$ in [6] to study the stability of nerve impulses. Evans and Feroe [7] numerically studied the linear stability of nerve impulse solutions of the Hodgkin-Huxley equations, by computing $D(\lambda)$ and locating its zeros using the argument principle. This is the method we shall use below. Recently, Swinton and Elgin [19] have used the same approach to study numerically the linear stability of laser pulses. Evans' function $D(\lambda)$ has also been used in a number of theoretical studies of traveling wave stability: for nerve impulses [6,11,25], singularly perturbed reaction diffusion systems [1,8], flame fronts [20], and solitary waves [17].

In [17], the generalized KdV-Burgers equation (1.1) was also considered. We now summarize the results of [17] that describe $D(\lambda)$ and its properties, for the traveling waves of (1.1).

If λ is an eigenvalue of $\mathcal{A}$ with corresponding L^2-eigenfunction $Y(\xi)$, then Y is a solution of the differential equation

$$\partial_\xi(-\partial_\xi^2 + \alpha\partial_\xi + c - \phi(\xi)^p)Y(\xi) = \lambda Y(\xi) \ . \tag{3.1}$$

As ξ tends to $\pm\infty$ respectively, the coefficients of (3.1) tend to those of the corresponding constant coefficient equations

$$\partial_\xi(-\partial_\xi^2 + \alpha\partial_\xi + c)Y(\xi) = \lambda Y(\xi) \ , \tag{3.2}$$

$$\partial_\xi(-\partial_\xi^2 + \alpha\partial_\xi + c - u_L^p)Y(\xi) = \lambda Y(\xi) \ . \tag{3.3}$$

These equations have solutions of the form $\exp(\mu\xi)$, where for (3.2) and (3.3) respectively, the exponent μ satisfies

$$\mathcal{P}_+(\mu) = \mu^3 - \alpha\mu^2 - c\mu + \lambda = 0 \ , \tag{3.4a}$$

$$\mathcal{P}_-(\mu) = \mu^3 - \alpha\mu^2 + pc\mu + \lambda = 0 \ . \tag{3.4b}$$

For an arbitrary $\lambda \in \Omega^+$, equations (3.4ab) respectively have roots $\mu_j^\pm(\lambda)$, $j = 1,2,3$, which satisfy

$$Re\,\mu_1^\pm(\lambda) < 0 < Re\,\mu_j^\pm(\lambda) \ , \quad j = 2,3 \ . \tag{3.5}$$

Corresponding to the solution $\exp(\mu_1^+\xi)$ of (3.2), which decays to zero as $\xi \to +\infty$, equation (3.1) has a solution $Y^+(\xi,\lambda)$, which is analytic in λ and satisfies

$$Y^+(\xi,\lambda) \sim \exp(\mu_1^+\xi) \qquad \text{as } \xi \to +\infty \ . \tag{3.6}$$

From this solution $Y^+(\xi,\lambda)$, one can define a function $D(\lambda)$, which is a sort of *transmission coefficient*, with the property that

$$Y^+(\xi,\lambda) \sim D(\lambda)\exp(\mu_1^-\xi) \qquad \text{as } \xi \to -\infty \ . \tag{3.7}$$

$D(\lambda)$ is an analytic function in Ω^+. If $D(\lambda) = 0$ for $\lambda \in \Omega^+$, then $Y^+(\xi,\lambda)$ must decay exponentially as $\xi \to -\infty$. In this case, λ is an eigenvalue of (3.1) with corresponding eigenfunction $Y^+(\xi,\lambda)$. Conversely, if λ is an eigenvalue with corresponding eigenfunction $Y(\xi)$, then $Y(\xi)$ must be a constant multiple of $Y^+(\xi,\lambda)$ and so $D(\lambda) = 0$, since $Y(\xi)$ is bounded on $\mathbb{R}$.

Theorem 3.1 *For $\lambda \in \Omega^+$, λ is an eigenvalue of $\mathcal{A}$ if and only if $D(\lambda) = 0$.*

The origin $\lambda = 0$ is an eigenvalue of $\mathcal{A}$ embedded in the essential spectrum, with eigenfunction $\partial_\xi\phi$. It is useful to observe that $D(\lambda)$ is naturally defined, by the same formula (3.7), on a larger domain $\Omega \supset \Omega^+$, defined by the requirements

$$Re\,\mu_1^\pm(\lambda) < Re\,\mu_j^\pm(\lambda) \ , \qquad j = 2,3 \ . \tag{3.8}$$

These inequalities hold in a region contained in Ω of the form $\{z : Re\, z > -\epsilon_0\}$, for some $\epsilon_0 > 0$ depending on α, c and p. Moreover $D(0) = 0$, since

$$\mu_1^-(0) = 0\ , \quad \mu_j^-(0) = \tfrac{1}{2}(\alpha \pm i\sqrt{4pc - \alpha^2})\ , \quad j = 2, 3\ ,$$

$$\mu_1^+(0) = \tfrac{1}{2}(\alpha - \sqrt{\alpha^2 + 4c}) < \mu_2^+(0) = 0 < \mu_3^+(0) = \tfrac{1}{2}(\alpha + \sqrt{\alpha^2 + 4c})\ .$$

Since $\lambda = 0$ is the site of transition to instability for gKdV as p increases through the critical value $p_c = 4$, it is natural to search for transitions to instability as $\alpha \downarrow 0$ with $p > 4$ by looking for eigenvalues emerging from $\lambda = 0$. However, this scenario was precluded by the following result proved in [17].

Propostion 3.2 *For any $\alpha > 0$, $p \geq 1$, $c > 0$, we have: (1) $D(0) = 0$, (2) $D'(0) \neq 0$.*

Thus, the expected onset of instability for fixed $p > 4$ and $\alpha \downarrow 0$ cannot be due to the motion of an eigenvalue through $\lambda = 0$; this would imply that for some $\alpha_* > 0$, the value $\lambda = 0$ would be a zero of $D(\lambda)$ of multiplicity greater than one, so that $D'(0) = 0$.

The result of Proposition 3.2 motivates us to search computationally for complex zeros of $D(\lambda)$ crossing into the right half plane as α decreases. In section 4, we will use the argument principle to count the number of zeros of $D(\lambda)$ in the right half plane. For that purpose, the following result, proved in the Appendix, will be useful:

Propostion 3.3 *As $|\lambda| \to \infty$ with $\lambda \in \Omega^+$, $D(\lambda) \to 1$.*

We now discuss the original characterization of $D(\lambda)$ given by Evans [6], which leads to a more efficient algorithm for computing $D(\lambda)$ than is suggested by (3.7). To describe this characterization, we follow the development of of [17].

First, write (3.1) as a system of three first order ODE's, using the standard reduction: $y = (Y, Y', Y'')^t$. We have

$$\frac{dy}{d\xi} = A(\xi, \lambda)\, y\ ,$$

where

$$A(\xi, \lambda) = \begin{pmatrix} 0 & 1 & 0 \\ 0 & 0 & 1 \\ -\lambda - \partial_\xi \phi(\xi)^p & c - \phi(\xi)^p & \alpha \end{pmatrix}. \tag{3.9}$$

We are also interested in the adjoint equation:

$$\frac{dz}{d\xi} = -z\,A(\xi,\lambda)\ , \tag{3.10}$$

where $z(\xi)$ is a 3-component row vector. The quantities $\mu_j^{\pm}(\lambda)$ in (3.5) are eigenvalues of the asymptotic matrices

$$A^{\pm}(\lambda) = \lim_{\xi\to\pm\infty} A(\xi,\lambda)\ .$$

The inequality (3.8) ensures the existence of solutions $\zeta^+(\xi,\lambda)$ of (3.9) and $\eta^-(\xi,\lambda)$ of (3.10), analytic in λ for $\lambda\in\Omega$, such that

$$\zeta^+(\xi,\lambda) \sim \exp(\mu_1^+\xi)\,v^+ \quad \text{as } \xi\to\ +\infty\ , \tag{3.11}$$

$$\eta^-(\xi,\lambda) \sim \exp(-\mu_1^-\xi)\,w^- \quad \text{as } \xi\to\ -\infty\ . \tag{3.12}$$

Here we make use of the definitions

$$v^+ = \begin{pmatrix} 1 \\ \mu_1^+ \\ (\mu_1^+)^2 \end{pmatrix}, \quad v^- = \begin{pmatrix} 1 \\ \mu_1^- \\ (\mu_1^-)^2 \end{pmatrix}, \tag{3.13}$$

$$w^+ = \Big(\mu_1^+(\mu_1^+-\alpha)-c,\ \mu_1^+-\alpha,\ 1\Big)/\mathcal{P}'_+(\mu_1^+)\ , \tag{3.14a}$$

and

$$w^- = \Big(\mu_1^-(\mu_1^--\alpha)+pc,\ \mu_1^--\alpha,\ 1\Big)/\mathcal{P}'_-(\mu_1^-)\ , \tag{3.14b}$$

which satisfy

$$(A^{\pm}-\mu_1^{\pm}I)v^{\pm}=0\ ,\quad w^{\pm}(A^{\pm}-\mu_1^{\pm}I)=0\ ,\quad w^+v^+=w^-v^-=1. \tag{3.15}$$

If y and z are any solutions to (3.9) and (3.10), then it is easy to check that $z\cdot y$ is independent of ξ. Using the particular choices $z=\eta^-(\xi,\lambda)$, and $y=\zeta^+(\xi,\lambda)$, we have using Proposition 1.4 of [17] that

$$\zeta^+(\xi,\lambda) \sim (\eta^-\cdot\zeta^+)(\lambda)\exp(\mu_1^-\xi)\,v^-(\lambda) \quad \text{as } \xi\to-\infty\ . \tag{3.16}$$

Comparison of the first component of (3.16) with (3.7) yields the formula

$$D(\lambda) = (\eta^-\cdot\zeta^+)(\lambda)\ . \tag{3.17}$$

4. Computational search for eigenvalues

Our strategy is summarized as follows: By Theorem 3.1, the search for eigenvalues of $\mathcal{A}$, the operator in (2.1), is reduced to the search for zeros of $D(\lambda)$. Zeros of $D(\lambda)$ in the right half plane can be counted using the argument principle. Since for $Re\,\lambda \geq 0$, $D(\lambda) \to 1$ as $|\lambda| \to \infty$, it follows that the number of zeros in the right half plane is determined by the number of times the image of the imaginary axis $\{z : z = it, t \in \mathbb{R}\}$ under $D(\cdot)$ wraps around the origin. Taking into account that this axis contains $\lambda = 0$, a simple zero of $D(\lambda)$, we find the following expression for n^+, the number of zeros of $D(\lambda)$ with $Re\,\lambda > 0$:

$$n^+ = -\frac{1}{2\pi}\int_{-\infty}^{+\infty} \frac{D'(it)}{D(it)}dt - \frac{1}{2}\ . \tag{4.1}$$

The quantity $n^+ + \frac{1}{2}$ is the winding number of the curve $t \mapsto D(-it)$, $-\infty < t < +\infty$, with respect to the origin. This is the image under $D(\cdot)$ of the imaginary axis oriented in the positive sense relative to the right half plane. Since $\overline{D(\lambda)} = D(\overline{\lambda})$, this can be expressed in terms of the change in the argument of $D(it)$, as t varies from 0^+ to $+\infty$;

$$n^+ = \frac{1}{\pi}[\ \arg D(+i\cdot 0) - \arg D(+i\cdot\infty)\ ] - \frac{1}{2} \tag{4.2}$$

Our numerical strategy to evaluate n^+ is to evaluate $D(it)$ for values of t ranging from .005 to 300000, minimizing computation by adaptively changing the increment in t, while keeping the angle between successive segments within prescribed bounds. The argument of $D(it)$ is updated from step to step, so that n^+ can be evaluated using formula (4.2) at the end of the computation.

For computing, we introduce the variable $v(\xi,\lambda) = \exp(-\mu_1(\xi,\lambda)\xi)\,\zeta^+(\xi,\lambda)$, cf. (3.9), where

$$\mu_1(\xi,\lambda) = \begin{cases} \mu_1^+ & \text{for } \xi > 0\ , \\ \mu_1^- & \text{for } \xi < 0\ . \end{cases} \tag{4.3}$$

The function $v(\xi,\lambda)$ satisfies

$$\frac{dv}{d\xi} = (A(\xi,\lambda) - \mu_1 I)v\ , \tag{4.4}$$

$$v(\xi,\lambda) \to \begin{cases} v^+ & \text{as } \xi \to +\infty\ , \\ D(\lambda)v^- & \text{as } \xi \to -\infty\ . \end{cases} \tag{4.5}$$

Let $w(\xi,\lambda) = \exp(\mu_1(\xi,\lambda)\xi)\,\eta^-(\xi,\lambda)$. Then, $D(\lambda) = w \cdot v$ and w satisfies

$$\frac{dw}{d\xi} = -w(A(\xi,\lambda) - \mu_1 I)\ , \qquad w(\xi,\lambda) \to w^- \quad \text{as } \xi \to -\infty.$$

To approximate $D(\lambda)$ numerically, we fix $\xi_+ > 0$ large, and solve (4.4) by a 4-th order Runge-Kutta method, setting $v(\xi_+) = v^+$. The system (4.4) is solved simultaneously with the system describing the wave profile, $\phi(\xi)$:

$$\frac{d\phi}{d\xi} = \psi\ , \qquad \frac{d\psi}{d\xi} = \alpha\psi + c\phi - \frac{1}{p+1}\phi^{p+1}\ . \tag{4.6}$$

Since from (1.6), $(\phi,\psi) \sim e^{\nu(\xi-\xi_0)}(1,\nu)$ as $\xi \to +\infty$, we fix the phase of the wave by setting $\xi_0 = 0$ and approximate by imposing the initial condition

$$(\phi(\xi_+),\psi(\xi_+)) = \exp(\nu\xi_+)(1,\nu)\ . \tag{4.7}$$

The direction of decreasing ξ is the stable direction for integrating (4.4) and (4.6), in order to approximate the stable manifold of the saddle point $(0,0)$ in (4.6), and to compute the solution spanning the stable subspace for system (4.4). We integrate (4.4) and (4.6) for $\xi_+ > \xi > \xi_-$, where $\xi_- < 0$ is sufficiently large so that $(\phi(\xi_-),\psi(\xi_-))$ is approximately equal to $(u_L,0)$. When this holds, $w(\xi_-,\lambda) \sim w^-$, and therefore $D(\lambda)$ is given approximately by

$$D(\lambda) \sim w^- \cdot v(\xi_-,\lambda). \tag{4.8}$$

Remark: The approximation (4.8) turns out to be rather better than the approximation $D(\lambda) \sim v_1(\xi_-,\lambda)$ suggested by (4.5). Apparently, this is because the rate of convergence in (4.5) as $\xi \to -\infty$ can be rather slow. But the slowly decaying components of $v(\xi,\lambda)$ are orthogonal to $w(\xi,\lambda)$, so are eliminated by (4.8) if the approximation $w(\xi_-,\lambda) \sim w^-$ is good. In Table 1 we list some computed values of $v_1(\xi)$ and $w^- \cdot v(\xi)$ for parameters near the transition to instablity: $p = 6$, $c = 1$, $\alpha = .074$, $\lambda = 2i$. Discretization error is estimated to be of the order of 10^{-7} for this computation, which was performed with $\xi_+ = 5$, and step size $\Delta\xi = .01$.

ξ	$\phi(\xi)$	$v_1(\xi)$	$w^- v(\xi)$
-200.0	1.38278	$-0.017043 - 0.002920i$	$-0.011739 - 0.000313i$
-200.2	1.38277	$-0.015799 + 0.003097i$	$-0.011738 - 0.000305i$
-200.4	1.38283	$-0.012580 + 0.007822i$	$-0.011729 - 0.000301i$
-200.6	1.38295	$-0.008514 + 0.009940i$	$-0.011718 - 0.000306i$
-200.8	1.38310	$-0.005081 + 0.008994i$	$-0.011712 - 0.000314i$
-201.0	1.38325	$-0.003600 + 0.005495i$	$-0.011709 - 0.000318i$
-201.2	1.38335	$-0.004763 + 0.000719i$	$-0.011705 - 0.000314i$
-201.4	1.38340	$-0.008376 - 0.003739i$	$-0.011698 - 0.000306i$
-201.6	1.38337	$-0.013406 - 0.006497i$	$-0.011692 - 0.000301i$
-201.8	1.38327	$-0.018304 - 0.006832i$	$-0.011695 - 0.000303i$
-202.0	1.38313	$-0.021513 - 0.004883i$	$-0.011708 - 0.000307i$
-202.2	1.38299	$-0.021980 - 0.001563i$	$-0.011725 - 0.000309i$
-202.4	1.38287	$-0.019498 + 0.001798i$	$-0.011736 - 0.000308i$
-202.6	1.38280	$-0.014779 + 0.003924i$	$-0.011736 - 0.000305i$
-202.8	1.38280	$-0.009226 + 0.004046i$	$-0.011728 - 0.000307i$
-203.0	1.38287	$-0.004484 + 0.002154i$	$-0.011720 - 0.000311i$
-348.6	1.38309	$-0.011683 - 0.000314i$	$-0.011714 - 0.000309i$
-348.8	1.38309	$-0.011696 - 0.000334i$	$-0.011714 - 0.000309i$
-349.0	1.38309	$-0.011716 - 0.000345i$	$-0.011714 - 0.000309i$
-349.2	1.38309	$-0.011737 - 0.000343i$	$-0.011714 - 0.000309i$
-349.4	1.38309	$-0.011750 - 0.000331i$	$-0.011714 - 0.000309i$
-349.6	1.38309	$-0.011753 - 0.000312i$	$-0.011714 - 0.000309i$
-349.8	1.38309	$-0.011743 - 0.000294i$	$-0.011714 - 0.000309i$
-350.0	1.38309	$-0.011724 - 0.000282i$	$-0.011714 - 0.000309i$

TABLE 1. Comparison of two approximations of $D(\lambda)$.

Numerical Results:

In our numerical computations, we fix $c = 1$, so $u_L = (p+1)^{\frac{1}{p}}$. Results for other values of c may be recovered from the scaling satisfied by the wave profile, namely

$$\phi(\xi, c, p, \alpha) = c^{\frac{1}{p}} \phi(c^{\frac{1}{2}}\xi, 1, p, c^{-\frac{1}{2}}\alpha) \; . \tag{4.9}$$

In figure 4 we plot $\pi^{-1} \arg D(it)$ vs t for $p = 6$ and the cases $\alpha = .074$ (dashed line) and $\alpha = .077$ (dash-dot). From (4.2), for $\alpha = .077$ we find $n^+ = 0$, i.e., there are no eigenvalues of positive real part. But for $\alpha = .074$, we find $n^+ = 2$ indicating that there are 2 eigenvalues of positive real part.

INSERT near here

Figure 4: $\pi^{-1} \arg D(it)$ vs t for $p = 6$, $\alpha = .074$ (dash), $\alpha = .077$ (dash-dot).

Figure 5 shows a portion of the curve $t \mapsto D(it)$, $-\infty < t < \infty$, for the cases (a) $\alpha = .077$, and (b) $\alpha = .074$. As α decreases from $\alpha = .077$ to $\alpha = .074$, we see that the loops around $\lambda = 0$ in figure 5(a) deform, so that they no longer pass around $\lambda = 0$ in figure 5(b). The rest of the curve changes little from case (a) to case (b), so we see that the total change in the winding number in (4.1) is +2 as α decreases from .077 to .074.

INSERT near here

Figure 5: The curve $D(it)$ near the origin, for $p = 6$.
(a) $\alpha = .077$, (b) $\alpha = .074$.

In Figure 6, we plot the image under $D(\cdot)$ of the upper half of the imaginary axis, the curve $t \mapsto D(it)$, $0 < it < \infty$. Because of the large variation in the magnitude of $D(it)$ (see Figure 7), the tenth root of the magnitude is taken; thus Figure 6 is a polar plot of $|D(it)|^{1/10}$ vs $\arg D(it)$. The large spike in the magnitude of $D(it)$ appears to be associated with proximity to the point λ_* on the boundary of the domain Ω where $\mu_1^-(\lambda_*) = \mu_2^-(\lambda_*)$. Since $\mathcal{P}'_-(\mu) = 0$ at this point, one finds that

$$\lambda_* = -\mu^3 + \alpha\mu^2 - p\mu \ , \quad \text{where} \quad \mu = \mu_1^-(\lambda_*) = (\alpha + i\sqrt{3p - \alpha^2})/3 \ .$$

This point is plotted as a diamond in Figure 3; it is close to the curve S_e^- because α is small.

INSERT near here

Figure 6: The curve $D(it)$, for $p = 6$, $\alpha = .074$.
The magnitude $|D(it)|$ is scaled by taking the tenth root.

INSERT near here

Figure 7: $\log_{10} |D(it)|$ vs t for $p = 6$, $\alpha = .074$.

For $p = 6$, the transition to instability occurs at approximately $\alpha = .075596$. The eigenvalues cross the imaginary axis at approximately $\lambda = \pm 2.0695i$. We also computed that a second pair of eigenvalues cross into the right half plane at $\alpha = .03657$, with $\lambda = \pm 2.2579i$. There is evidence that a third pair crosses as α is decreased further. (We

might conjecture that, given any N, there is an α_N such that for $\alpha < \alpha_N$, N pairs of eigenvalues have crossed into the right half plane, with $\alpha_N \to 0$ as $N \to \infty$.)

We plot in figure 8 some parts of the curves α vs p along which the real part of some eigenvalue is zero. The upper curve marks the neutral stability curve $\alpha = \alpha_0(p)$, across which the transition to instability occurs: n^+ jumps from 0 to 2 as α decreases across this curve. Across the lower curve $\alpha = \alpha_1(p)$, n^+ jumps from 2 to 4; a second complex conjugate pair of eigenvalues has crossed the imaginary axis.

INSERT near here

Figure 8: Transition curves, where $Re\,\lambda = 0$ for some eigenvalue.

As p decreases toward the value 4, the value of $\alpha = \alpha_0(p)$ along the neutral stability curve also decreases, as does the value of $\alpha = \alpha_1(p)$ along the second transition curve. Our numerical results are consistent with the hypothesis that $\alpha_0(p) \to 0$ as $p \downarrow 4$. It appears that the traveling wave $\phi(x - ct)$ is linearly stable for any $\alpha > 0$ when $p < 4$ (the regime where the solitary wave $\phi_0(x - ct)$ is stable). In figure 9 we plot $\log \alpha_j(p)$ vs $\log(p - 4)$. We find that these graphs are nearly linear, with slope approaching $+\frac{3}{2}$ as $p \to 4^+$. Thus it appears that

$$\alpha_j(p) \sim K_j \cdot (p-4)^{3/2} \quad \text{as } p \to 4^+ \,, \tag{4.10}$$

where K_0 is approximately .031, and K_1 is approximately .014.

INSERT near here

Figure 9: Transition curves $\alpha_j(p)$ vs $p - 4$, log-log plot.

5. Dynamic simulations

We have performed numerical computations of solutions of the initial value problem for the generalized KdV-Burgers equation (1.1), with initial data close to a traveling wave, for parameter values near the transition to instability. The goal was to confirm the predictions of linear stability calculations in section 4, and to study the nature of the Hopf bifurcation suggested by the crossing of pairs of complex eigenvalues into the right half plane.

In order to describe the numerical scheme we used, first consider the evolution equation for the perturbation of the wave, $v(x-ct,t) = u(x,t) - \phi(x-ct)$, namely

$$\begin{aligned} \partial_t v &= -\partial_\xi^3 v + \alpha \partial_\xi^2 v + c\partial_\xi v - \partial_\xi g(\xi, v) \\ &= \mathcal{A}_+ v - \partial_\xi g(\xi, v) \ , \end{aligned} \tag{5.1}$$

where

$$g(\xi, v) = \frac{1}{p+1}[\ (\phi(\xi)+v)^{p+1} - \phi(\xi)^{p+1}\ ] \ .$$

We approximate the solution of (5.1) using Strang splitting [18]; in particular we solve with alternating fractional time steps of length Δt the equations

$$\partial_t v = \mathcal{A}_+ v \ , \tag{5.2}$$

$$\partial_t v + \partial_\xi g(\xi, v) = 0 \ , \tag{5.3}$$

taking half-steps of length $\Delta t/2$ at the beginning and end. We solve the equation (5.2) on a large finite interval $[\xi_-, \xi_+] = [-300, 20]$, using centered differences in ξ, and a Crank-Nicholson discretization in time. We used 25600 grid points in space, with time step $\Delta t = .0005$. The boundary conditions imposed correspond to $v(\xi_-) = 0$, $v(\xi_+) = 0$, and $\partial_\xi v(\xi_+) = 0$. Equation (5.3) was solved using a Lax-Wendroff method [14]. The overall scheme is formally second order accurate in space and time.

Computations were performed for $p = 6$ and $\alpha = .05$ fixed, varying c near the value $c_{cr} \sim .438$, at which the transition to instability occurs. At this transition, a critical eigenvalue $\lambda_0(c)$ crossed into the right half plane, with $\lambda_0(c_{cr}) \sim .600i$.

For each calculation, the initial data was chosen as a small multiple of the eigenfunction corresponding to the critical eigenvalue:

$$v(\xi, 0) = \epsilon Re\, Y^+(\xi, \lambda_*(c_{cr})) \tag{5.4}$$

for some $\epsilon > 0$. The real and imaginary parts of the eigenfunction $Y^+(\xi, \lambda_*(c_{cr}))$ at transition are plotted in figure 10.

INSERT near here

Figure 10. Real (top) and imaginary (bottom) parts of the critical eigenfunction.

Results appear in figures 11-16. For $c = .41$, the critical eigenvalue $\lambda(.41) \sim -.00777 + .553i$. Choosing $\epsilon = 10^{-5}$, the L^2-norm of the solution for $0 < t < 50$ decayed toward zero at the rate $\exp(-.0075t)$, agreeing well with the rate predicted by the linear stability calculation.

But when the perturbation amplitude ϵ is increased beyond $\epsilon = .05$, decay is no longer observed; a nonlinear instability occurs. The L^2-norm of the perturbation grows, and a complicated transient ensues. (See Figure 11.)

INSERT near here

Figure 11. L^2-norm of v vs t, for $c = .41$, $\epsilon = .05$.

In Figures 12-13 appear results for the case $c = .438$, very close to but slightly above the predicted transition. As shown in Figure 12, for $\epsilon = 10^{-3}$ the L^2-norm of v is initially irregular, then increases monotonically. A plot of $v(\xi_0, t)$ for ξ_0 fixed appears in Figure 13.

INSERT near here

Figure 12. L^2-norm of v vs t, for $c = .438$, $\epsilon = .001$.

INSERT near here

Figure 13. $v(\xi_0, t)$ vs t, for $c = .438$, $\epsilon = .001$, $\xi_0 = -16$.

For $c = .47$ the wave appears to be unstable. When $\epsilon = 10^{-5}$, the growth rate again agrees well with linear prediction. Taking $\epsilon = .002$, and computing for $0 < t < 330$, the

perturbation is observed to grow to large amplitude. In Figure 14 we plot the L^2 norm of v vs t. In Figure 15, we plot $\partial_t v(\xi_0, t)$ vs. $v(\xi_0, t)$. In Figure 16, we plot $v(\xi, t)$ vs. ξ at integer times from $t = 319$ to 330. Time increases upwards. The horizontal axis runs from -300 to 20 and the snapshots are successively displaced one unit upward along the vertical axis. This sequence illustrates how the pertubation is evolving as its magnitude begins to be comparable to that of the wave profile. An instability grows out of the leading part of the wave, propagates backward along the profile, then dissipates as a new cycle begins.

INSERT near here

Figure 14. L^2 norm of $v(\cdot, t)$ vs t, for $c = .47$, $\epsilon = .002$.

INSERT near here

Figure 15. $\partial_t v(\xi_0, t)$ vs $v(\xi_0, t)$, for $c = .47$, $\epsilon = .002$.

INSERT near here

Figure 16. $v(\xi, t)$ vs ξ, for $c = .47$, $\epsilon = .002$, $t = 319, \ldots, 330$.

6. Conclusion

We have numerically investigated the stability of traveling wave solutions of the generalized KdV-Burgers equation (1.1), by finding eigenvalues using their characterization as zeros of Evans' function $D(\lambda)$, and by numeric integration of the initial value problem for perturbations of the wave.

To summarize the numerical evidence from section 4, a transition to linear instability takes place when:

(a) For fixed c and $p > 4$, α is made sufficiently small;

(b) For fixed α and $p > 4$, c is made sufficiently large.

The transition to instability occurs as a pair of complex conjugate eigenvalues crosses the imaginary axis into the right half plane. Additional pairs of complex eigenvalues cross into the right half plane as α is decreased or c is increased further. The neutral stability curve $\alpha = \alpha_0(p)$ is approximately described for p close to 4 by $\alpha_0(p) \sim .031(p-4)^{3/2}$.

The numerical evidence in section 5 strongly suggests that a subcritical Hopf bifurcation occurs as c increases near $c_{cr} = .438$ (with $\alpha = .05$ and $p = 6$ fixed). No stable time periodic solution is detected. While we are not aware that a Hopf bifurcation theorem has been proved for the equation (5.1) for the evolution of perturbations of the traveling wave, the numerical results are consistent with a classical description of a subcritical Hopf bifurcation in finite dimensions [15]. They suggest the existence of an unstable time periodic solution which exists for $c < c_{cr}$, whose unstable manifold, of dimension two, contains a component in which solution trajectories spiral toward the origin $v = 0$, and a component on which the perturbation v grows to large amplitude. Thus the basin of attraction of the wave ϕ shrinks as c approaches c_{cr}, vanishing entirely for $c > c_{cr}$, when small perturbations grow to large amplitude.

We do not have analytical results to support the numerical evidence, but it may be that in the limit $p \to 4$, $\alpha \to 0$, the eigenvalue problem may be accessible to analysis. The structure of the traveling wave can probably be well-characterized in that limit by studying the system (4.5) using the method of averaging and homoclinic bifurcation theory. (An asymptotic study was done for the KdV-Burgers equation with small α by Johnson [10].) More difficult (and interesting) would be characterizing Evans' function in the limit.

Appendix

Here we prove that $\lim_{\lambda\to\infty} D(\lambda) = 1$ for $\lambda \in \Omega_+$, which is Proposition 3.3. The proof relies on results contained in §1.7 of [17]. Below, the proof is sketched out; for full details the reader is referred to [17].

For $|\lambda|$ large with $\lambda \in \Omega_+$, we will see below that the asymptotic matrices $A^{\pm}(\lambda)$ are diagonalizable. Define $V^{\pm}(\lambda)$ to be the matrix of right eigenvectors of $A^{\pm}(\lambda)$, with components $V^{\pm}_{jk} = (\mu^{\pm}_k)^{j-1}$. Define $W^{\pm}(\lambda)$ to be the corresponding matrix of left eigenvectors, with $W^{\pm}V^{\pm} = I$, so that $B^{\pm}(\lambda) = W^{\pm}A^{\pm}V^{\pm} = \mathrm{diag}(\mu^{\pm}_1, \mu^{\pm}_2, \mu^{\pm}_3)$. is diagonal.

Define $p(\xi,\lambda) = W^+(\lambda)\zeta^+(\xi,\lambda)$, and $q(\xi,\lambda) = \eta^-(\xi,\lambda)V^-(\lambda)$. Then

$$dp/d\xi = B^+(\lambda)p + F^+(\xi,\lambda)p\ , \quad \xi > 0\ , \tag{A.1}$$

$$dq/d\xi = -qB^-(\lambda) - qF^-(\xi,\lambda)\ , \quad \xi < 0\ , \tag{A.2}$$

where it turns out that the components of $F^{\pm}(\xi,\lambda)$ are given by

$$F^{\pm}_{jk}(\xi,\lambda) = (\rho_0(\xi) + \mu^{\pm}_k(\lambda)\rho_1(\xi))/\mathcal{P}_{\pm}{}'(\mu^{\pm}_j(\lambda)) \ ,$$

with $\rho_0 = -\partial_\xi(\phi^p)$, $\rho_1 = -\phi^p$.

Now, from Proposition 1.17 and Corollary 1.19 of [17], we know that as $|\lambda| \to \infty$ with $\lambda \in \Omega_+$, $q(0,\lambda)$ is bounded and

$$p(0,\lambda) = W^+\zeta^+(0,\lambda) = e_1 + o(1) \ , \tag{A.3}$$

$$q(0,\lambda)\cdot e_1 = \eta^-(0,\lambda)V^- e_1 = 1 + o(1) \ , \tag{A.4}$$

where $e_1 = (1,0,0)^t$, provided the following are true for $i = 0, 1$:

$$|(\mu^{\pm}_k)^i/\mathcal{P}'_{\pm}(\mu^{\pm}_j)| \le C \qquad \text{for } j = 1,2,3,\ k = 2,3 \ , \tag{A.5}$$

$$|(\mu^{\pm}_1)^i/\mathcal{P}'_{\pm}(\mu^{\pm}_j)| = o(1) \quad \text{as } |\lambda| \to \infty, \text{ for } j = 1,2,3 \ . \tag{A.6}$$

To prove (A.5) and (A.6) we appeal to Lemma 1.20 of [17], and write

$$\mathcal{P}_{\pm}(\mu) = \tilde{\mathcal{P}}(\mu) + \mathcal{Q}_{\pm}(\mu) \ , \tag{A.7}$$

where

$$\tilde{\mathcal{P}}(\mu) = (\mu - \frac{\alpha}{3})^3 + \lambda \ ,$$

$$\mathcal{Q}_+(\mu) = (\alpha^2 - c)\mu + \alpha^3/27 \ , \quad \mathcal{Q}_-(\mu) = (\alpha^2 + pc)\mu + \alpha^3/27 \ .$$

It then follows from this Lemma that as $|\lambda| \to \infty$ with $\lambda \in \Omega_+$,

$$\mu^{\pm} = (-\lambda)^{1/3} + \frac{\alpha}{3} + O(|\lambda|^{-1/3}) \tag{A.8}$$

It is straightforward to see that (A.8) implies that for $i = 0, 1$,

$$|(\mu^{\pm}_k)^i/\mathcal{P}'_{\pm}(\mu^{\pm}_j)| = o(1) \quad \text{for } j,k = 1,2,3 \ ,$$

as $|\lambda| \to \infty$ with $\lambda \in \Omega_+$. Therefore (A.3) and (A.4) are true for the KdV-Burgers equation. From (A.8), one may also show that

$$V^+ = V^- \cdot (I + o(1)) \ , \tag{A.9}$$

since $V_{jk}^{\pm} = (\mu_k^{\pm})^{j-1}$. Combining (A.9) with (A.4) gives

$$\eta^-(0,\lambda)V^+e_1 = 1 + o(1) \ . \tag{A.10}$$

Now to prove $D(\lambda) \to 1$ as $|\lambda| \to \infty$ with $\lambda \in \Omega_+$, we recall from (3.17) that

$$D(\lambda) = \eta^- \cdot \zeta^+ = \eta^- V^+ \cdot W^+ \zeta^+ \ .$$

Then from (A.3) and (A.10) it is clear that $D(\lambda) = 1 + o(1)$.

REFERENCES

[1] Alexander, J., Gardner, R. and Jones, C.K.R.T., A topological invariant arising in the stability analysis of traveling waves, *J. Reine Angew. Math.* **410** (1990) 167–212.

[2] Benjamin, T.B., The stability of solitary waves, *Proc. R. Soc. Lond.* **A328** (1972) 153–183.

[3] Bona, J.L., On the stability of solitary waves, *Proc. R. Soc. Lond.* **A344** (1975) 363–374.

[4] Bona, J.L. and Schonbek, M.E., Traveling wave solutions to the Korteweg-de Vries-Burgers equation, *Proc. R. Soc. Edin.* **A101** (1985) 207–226.

[5] Bona, J.L., Souganidis, P.E., and Strauss, W.A., Stability and instability of solitary waves, *Proc. R. Soc. Lond.* **A411** (1987) 395–412.

[6] Evans, J.W., Nerve axon equations, IV: The stable and unstable impulse , *Indiana Univ. Math. J.* **24** (1975) 1169–1190.

[7] Evans, J.W. and Feroe J., Local stability theory of the nerve impulse, *Math. Biosci.* **37** (1977) 23–50.

[8] Gardner, R. and Jones, C.K.R.T., Traveling waves of a perturbed diffusion equation arising in a phase field model, *Ind. Univ. Math. J.* **38** (1989) 1197–1222.

[9] Henry, D., *Geometric Theory of Semilinear Parabolic Equations*, Lec. Notes in Math. **840**, Springer, New York, 1981.

[10] Johnson, R.S., A nonlinear equation incorporating damping and dispersion, *J. Fluid Mech.* **42** (1970) 49–60.

[11] Jones, C.K.R.T., Stability of the traveling wave solution to the FitzHugh-Nagumo equation, *Transactions Amer. Math. Soc.* **286** (1984) 431–469.

[12] Khodja, M., *Nonlinear stability of oscillatory traveling waves for some systems of hyperbolic conservation laws*, Ph. D. dissertation, University of Michigan, 1989.

[13] Laedke, E.W. and Spatschek, K.H., Stability theorem for KdV type equations, *J. Plasma Phys.* **32** (1984) 263–272.

[14] Lax, P., *Hyperbolic Systems of Conservation Laws and the Mathematical Theory of Shock Waves*, CBMS Lec. Notes **11**, SIAM, Philadelphia, 1973.

[15] Marsden, J. and McCracken, M., *The Hopf Bifurcation and its Applications*, Springer, New York, 1976.

[16] Pego, R.L., Remarks on the stability of shock profiles for conservation laws with dissipation, *Transactions Amer. Math. Soc.* **291** (1985) 353–361.

[17] Pego, R.L. and Weinstein, M.I., Eigenvalues, and solitary wave instabilities, *Phil. Trans. R. Soc. Lond.* **A340** (1992) 47–94.

[18] Strang, G., On the construction and comparison of difference schemes, *SIAM J. Num. Anal.* **5** (1968) 506–517.

[19] Swinton, J. and Elgin, J., Stability of travelling pulse to a laser equation, *Phys. Lett.* **A145** (1990) 428–433.

[20] Terman, D., Stability of planar wave solutions to a combustion model, *SIAM J. Math. Anal.* **21** (1990) 1139–1171.

[21] Weinstein, M.I., On the solitary traveling wave of the generalized Korteweg-de Vries equation, in *Nonlinear Systems of Partial Differential Equations in Applied Mathematics*, B. Nicolaenko, D. Holm, J. Hyman, eds., Lectures in Appl. Math. **23**, Amer. Math. Soc., 1986.

[22] Weinstein, M.I., Lyapunov stability of ground states of nonlinear dispersive evolution equations, *Comm. Pure Appl. Math.* **39** (1986) 51–68.

[23] Weinstein, M.I., Existence and dynamic stability of solitary wave solutions of equations arising in long wave propagation, *Comm. PDE* **12** (1987) 1133–1173.

[24] Whitham, G.B., *Linear and Nonlinear Waves*, Wiley-Interscience, New York, 1974.

[25] Yanagida, E., Stability of fast traveling pulse solutions of the Fitzhugh-Nagumo equations, *J. Math. Biol.* **22** (1985), 81–104.

REFERENCES

[1] Alexander, J., Gardner, R. and Jones, C.K.R.T., *J. Reine Angew. Math.* **410** (1990) 167.

[2] Benjamin, T.B., *Proc. R. Soc. Lond.* **A328** (1972) 153.

[3] Bona, J.L., *Proc. R. Soc. Lond.* **A344** (1975) 363.

[4] Bona, J.L. and Schonbek, M.E., *Proc. R. Soc. Edin.* **A101** (1985) 207.

[5] Bona, J.L., Souganidis, P.E., and Strauss, W.A., *Proc. R. Soc. Lond.* **A411** (1987) 395.

[6] Evans, J.W., *Indiana Univ. Math. J.* **24** (1975) 1169.

[7] Evans, J.W. and Feroe J., *Math. Biosci.* **37** (1977) 23.

[8] Gardner, R. and Jones, C.K.R.T., *Ind. Univ. Math. J.* **38** (1989) 1197.

[9] Henry, D., *Geometric Theory of Semilinear Parabolic Equations*, Lec. Notes in Math. **840**, Springer, New York, 1981.

[10] Johnson, R.S., *J. Fluid Mech.* **42** (1970) 49.

[11] Jones, C.K.R.T., *Transactions Amer. Math. Soc.* **286** (1984) 431.

[12] Khodja, M., Ph. D. dissertation, University of Michigan, 1989.

[13] Laedke, E.W. and Spatschek, K.H., *J. Plasma Phys.* **32** (1984) 263.

[14] Lax, P., *Hyperbolic Systems of Conservation Laws and the Mathematical Theory of Shock Waves*, CBMS Lec. Notes **11**, SIAM, Philadelphia, 1973.

[15] Marsden, J. and McCracken, M., *The Hopf Bifurcation and its Applications*, Springer, New York, 1976.

[16] Pego, R.L., *Transactions Amer. Math. Soc.* **291** (1985) 353.

[17] Pego, R.L. and Weinstein, M.I., *Phil. Trans. R. Soc. Lond.* **A340** (1992) 47.

[18] Strang, G., *SIAM J. Num. Anal.* **5** (1968) 506.

[19] Swinton, J. and Elgin, J., *Phys. Lett.* **A145** (1990) 428.

[20] Terman, D., *SIAM J. Math. Anal.* **21** (1990) 1139.

[21] Weinstein, M.I., in *Nonlinear Systems of Partial Differential Equations in Applied Mathematics*, B. Nicolaenko, D. Holm, J. Hyman, eds., Lectures in Appl. Math. **23**, Amer. Math. Soc., 1986.

[22] Weinstein, M.I., *Comm. Pure Appl. Math.* **39** (1986) 51.

[23] Weinstein, M.I., *Comm. PDE* **12** (1987) 1133.

[24] Whitham, G.B., *Linear and Nonlinear Waves*, Wiley-Interscience, New York, 1974.

[25] Yanagida, E., *J. Math. Biol.* **22** (1985), 81.

Figure Captions

Figure 1. Top: $\phi - \phi'$ phase plane. Bottom: $\phi(\xi)$ vs ξ.

Figure 2. Spectrum of $\mathcal{A}_0$ for (a) $p < 4$ and (b) $p > 4$.
Wavy line indicates essential spectrum covers imaginary axis.

Figure 3. Spectrum of $\mathcal{A}$ for (a) $\alpha = .08$, (b) $\alpha = .07$.

TABLE 1. Comparison of two approximations of $D(\lambda)$.

Figure 4: $\pi^{-1} \arg D(it)$ vs t for $p = 6$, $\alpha = .074$ (dash), $\alpha = .077$ (dash-dot).

Figure 5: The curve $D(it)$ near the origin, for $p = 6$.
(a) $\alpha = .077$, (b) $\alpha = .074$.

Figure 6: The curve $D(it)$, for $p = 6$, $\alpha = .074$.
The magnitude $|D(it)|$ is scaled by taking the tenth root.

Figure 7: $\log_{10} |D(it)|$ vs t for $p = 6$, $\alpha = .074$.

Figure 8: Transition curves, where $Re\lambda = 0$ for some eigenvalue.

Figure 9: Transition curves $\alpha_j(p)$ vs $p - 4$, log-log plot.

Figure 10. Real (top) and imaginary (bottom) parts of the critical eigenfunction.

Figure 11. L^2-norm of v vs t, for $c = .41$, $\epsilon = .05$.

Figure 12. L^2-norm of v vs t, for $c = .438$, $\epsilon = .001$.

Figure 13. $v(\xi_0, t)$ vs t, for $c = .438$, $\epsilon = .001$, $\xi_0 = -16$.

Figure 14. L^2 norm of $v(\cdot, t)$ vs t, for $c = .47$, $\epsilon = .002$.

Figure 15. $\partial_t v(\xi_0, t)$ vs $v(\xi_0, t)$, for $c = .47$, $\epsilon = .002$.

Figure 16. $v(\xi, t)$ vs ξ, for $c = .47$, $\epsilon = .002$, $t = 319, \ldots, 330$.

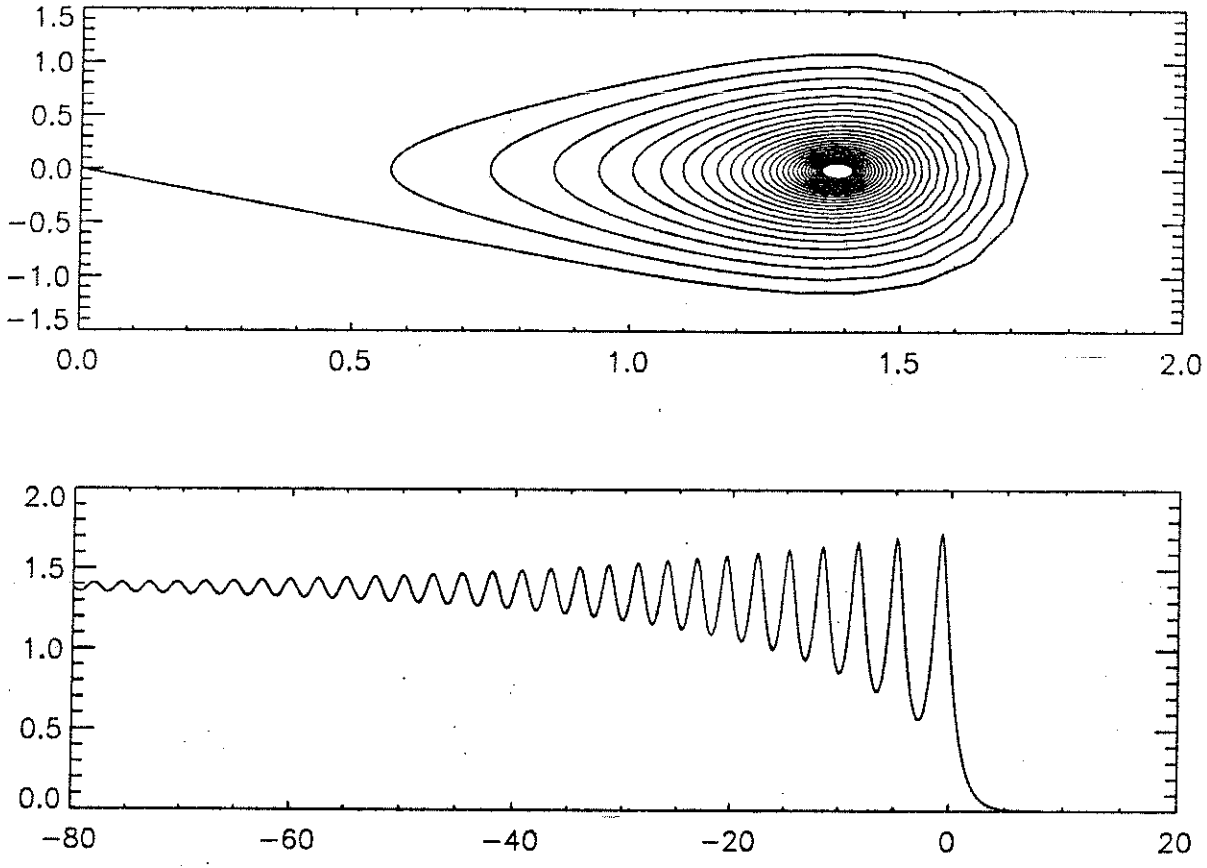

Figure 1. Top: $\phi - \phi'$ phase plane. Bottom: $\phi(\xi)$ vs ξ.

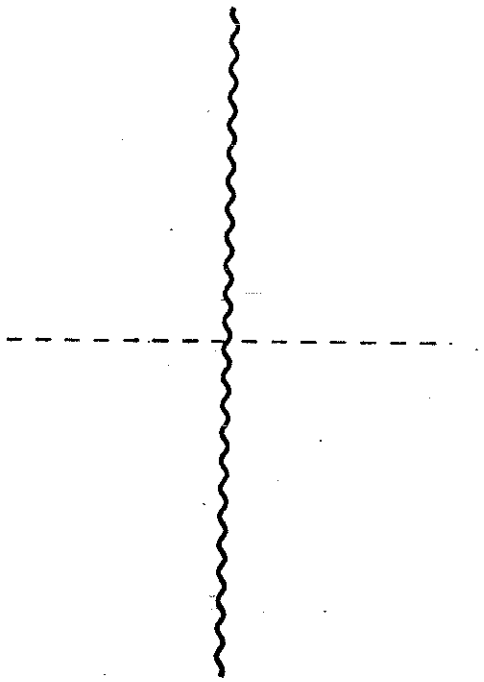

Figure 2 (a) p<4

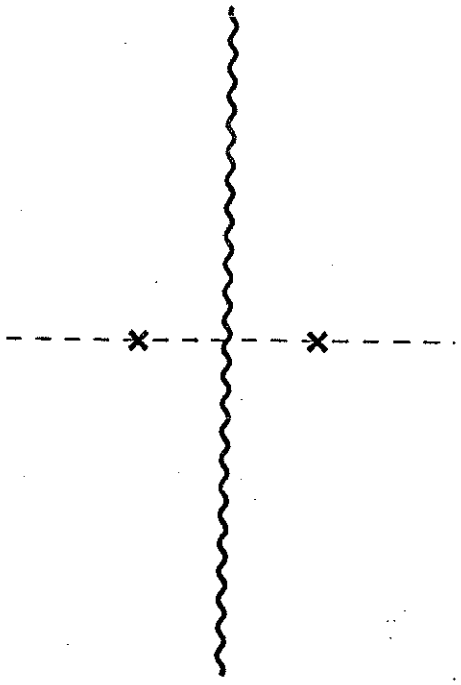

Figure 2 (b) p>4

Figure 2. Spectrum of $\mathcal{A}_0$ for (a) $p < 4$ and (b) $p > 4$.
Wavy line indicates essential spectrum covers imaginary axis.

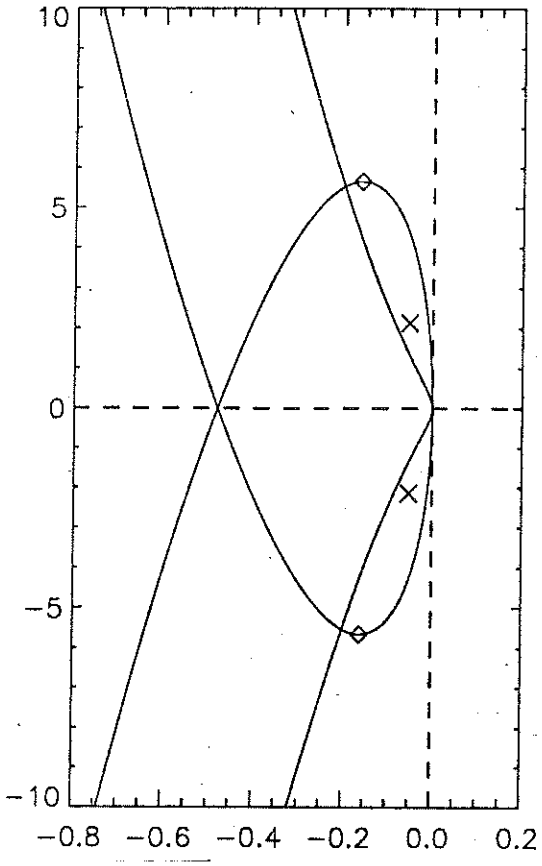

Figure 3 (a)

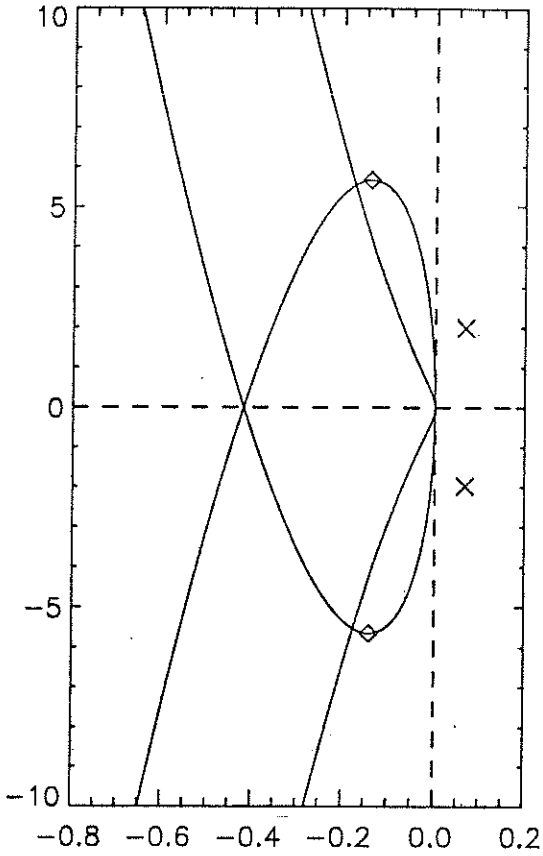

Figure 3 (b)

Figure 3. Spectrum of $\mathcal{A}$ for (a) $\alpha = .08$, (b) $\alpha = .07$.

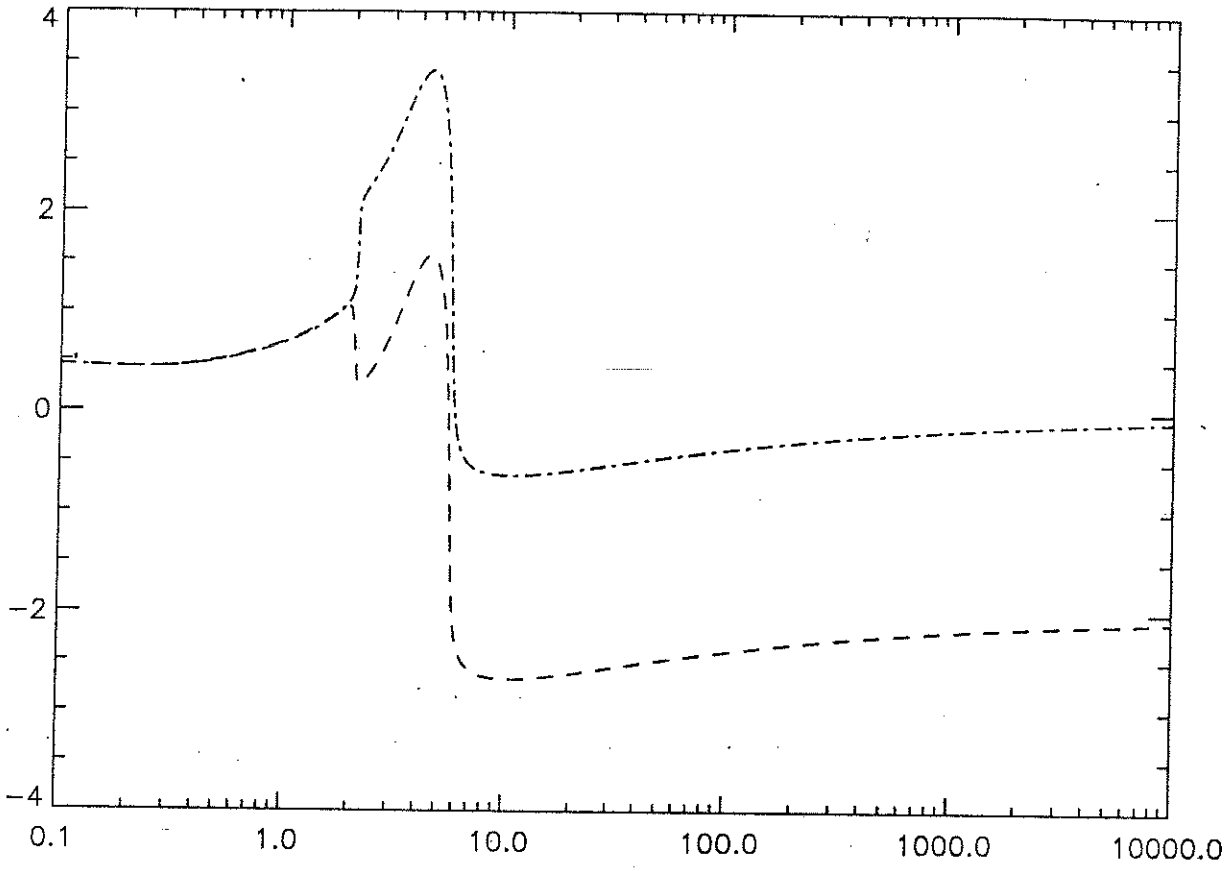

Figure 4

Figure 4: $\pi^{-1} \arg D(it)$ vs t for $p = 6$, $\alpha = .074$ (dash), $\alpha = .077$ (dash-dot).

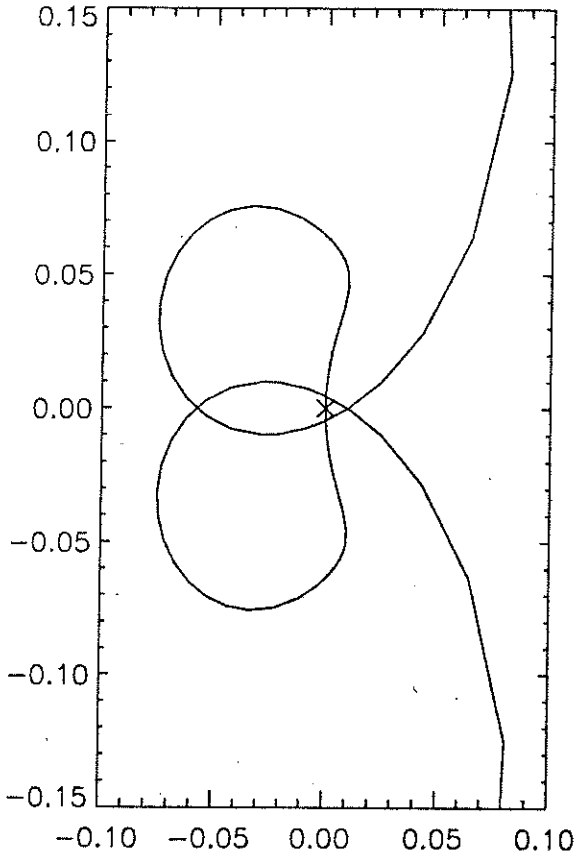

Figure 5 (a) alpha=.077

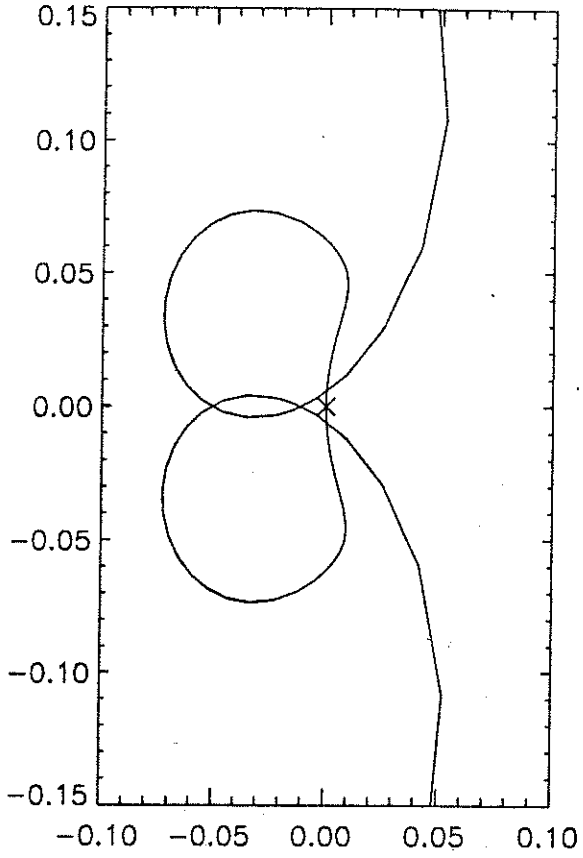

Figure 5 (b) alpha=.074

Figure 5: The curve $D(it)$ near the origin, for $p = 6$.
(a) $\alpha = .077$, (b) $\alpha = .074$.

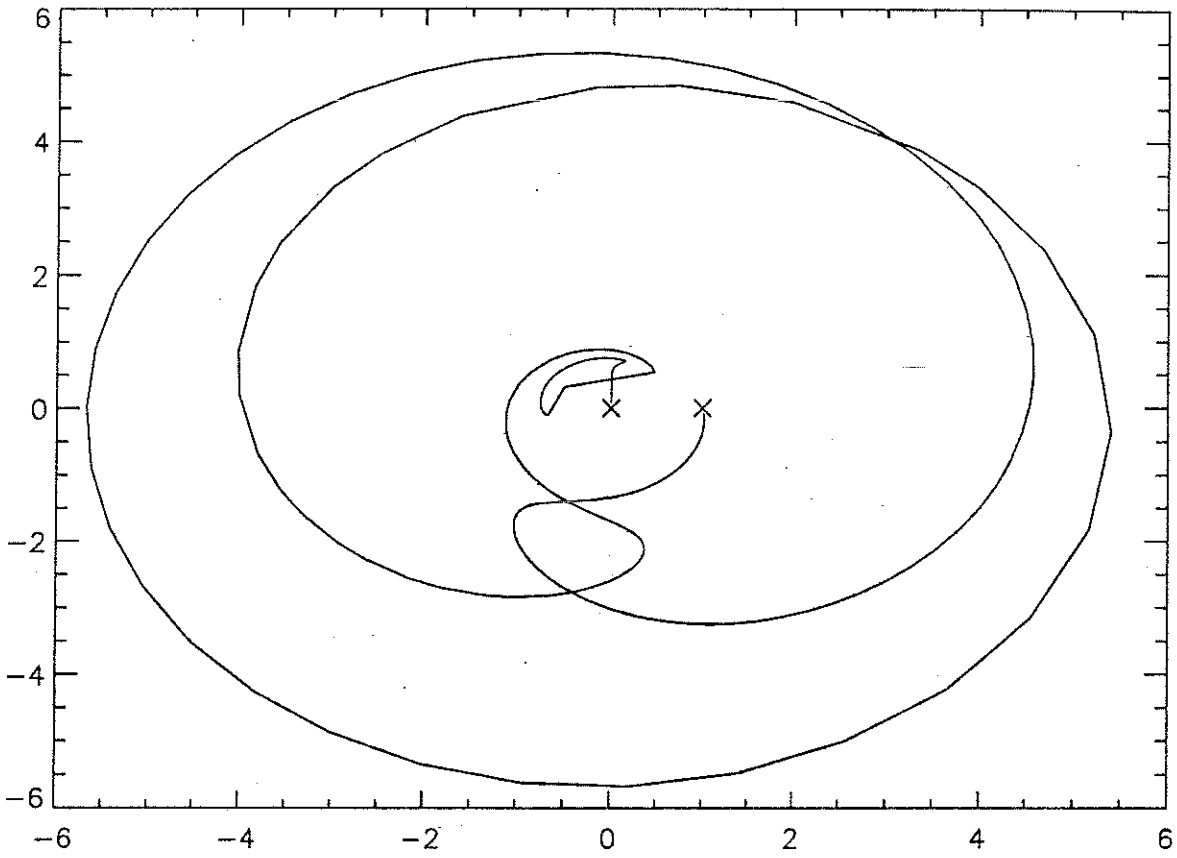

Figure 6

Figure 6: The curve $D(it)$, for $p = 6$, $\alpha = .074$.
The magnitude $|D(it)|$ is scaled by taking the tenth root.

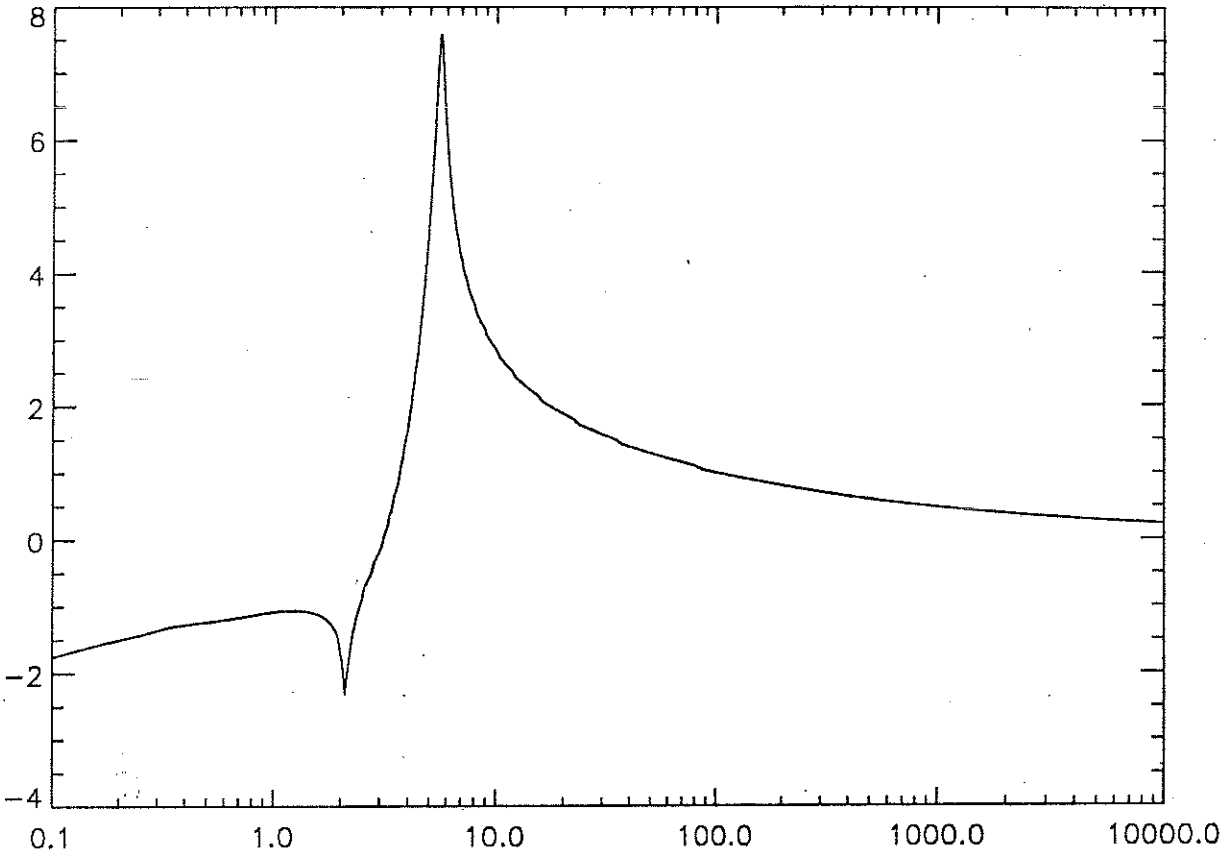

Figure 7: $\log_{10}|D(it)|$ vs t for $p = 6$, $\alpha = .074$.

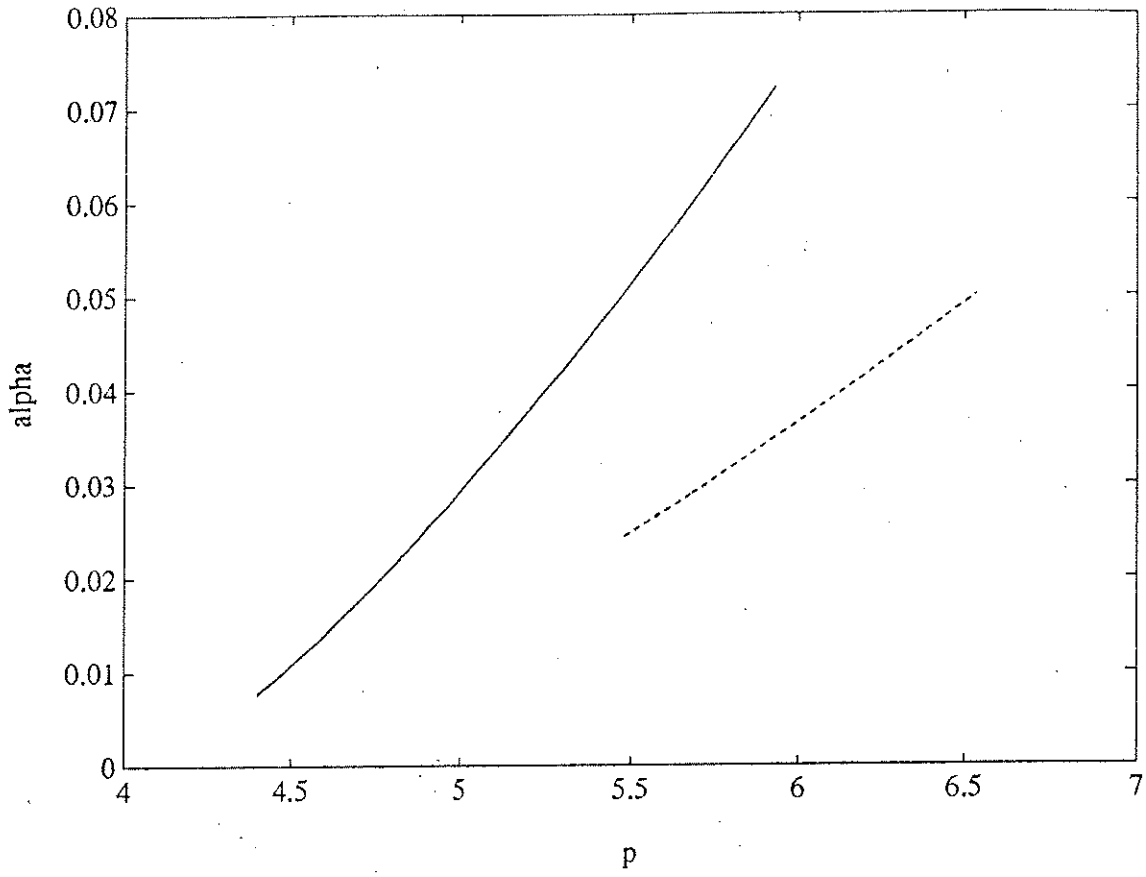

Figure 8: Transition curves, where $Re\lambda = 0$ for some eigenvalue.

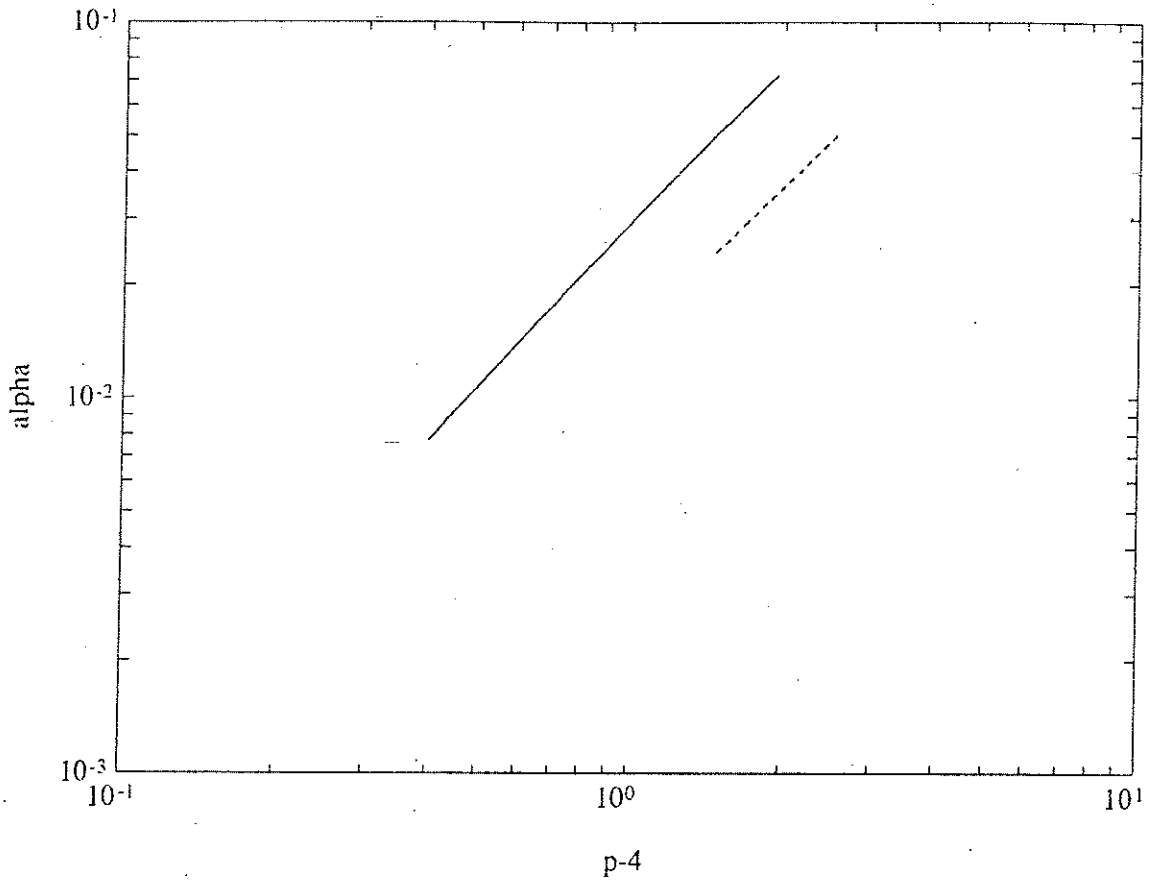

Figure 9: Transition curves $\alpha_j(p)$ vs $p-4$, log-log plot.

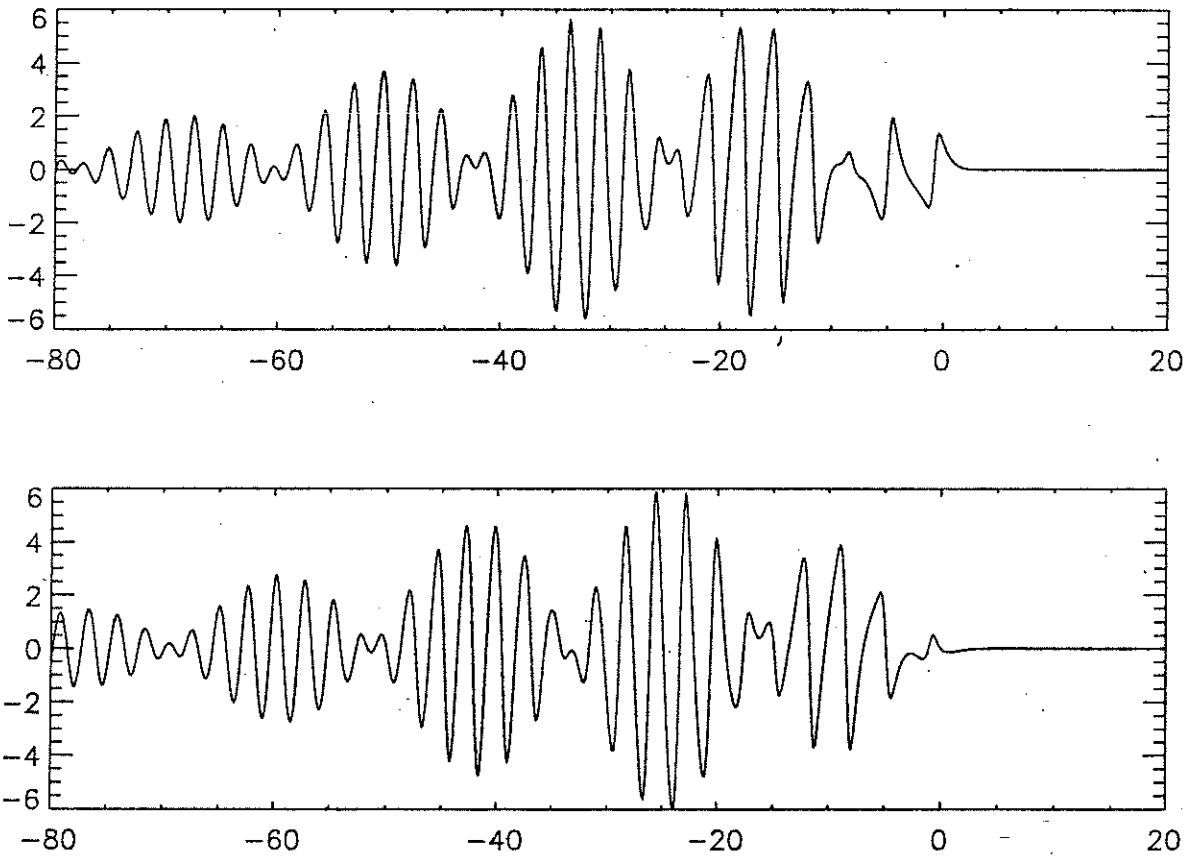

Figure 10. Real (top) and imaginary (bottom) parts of the critical eigenfunction.

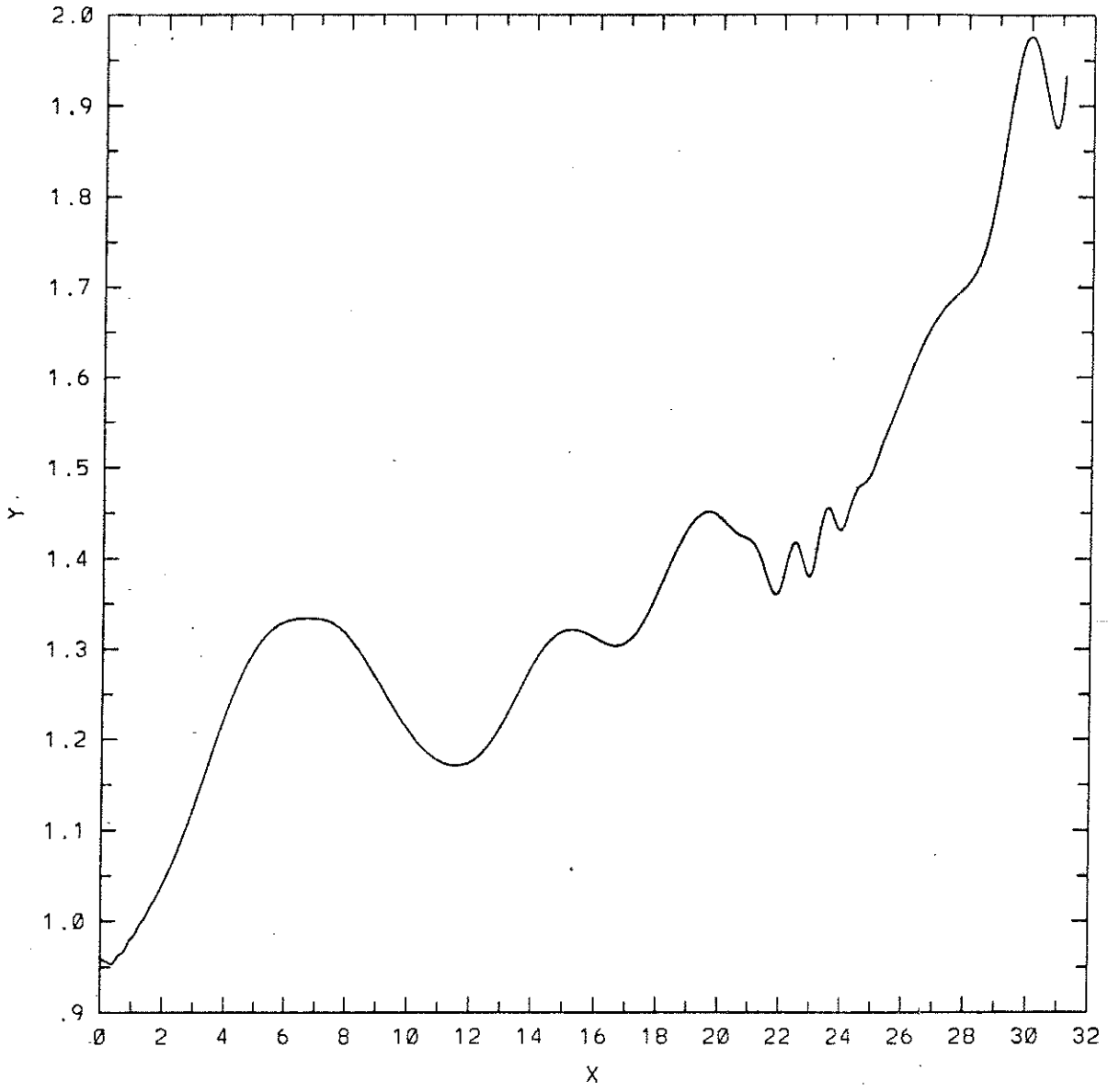

Figure 11. L^2-norm of v vs t, for $c = .41$, $\epsilon = .05$.

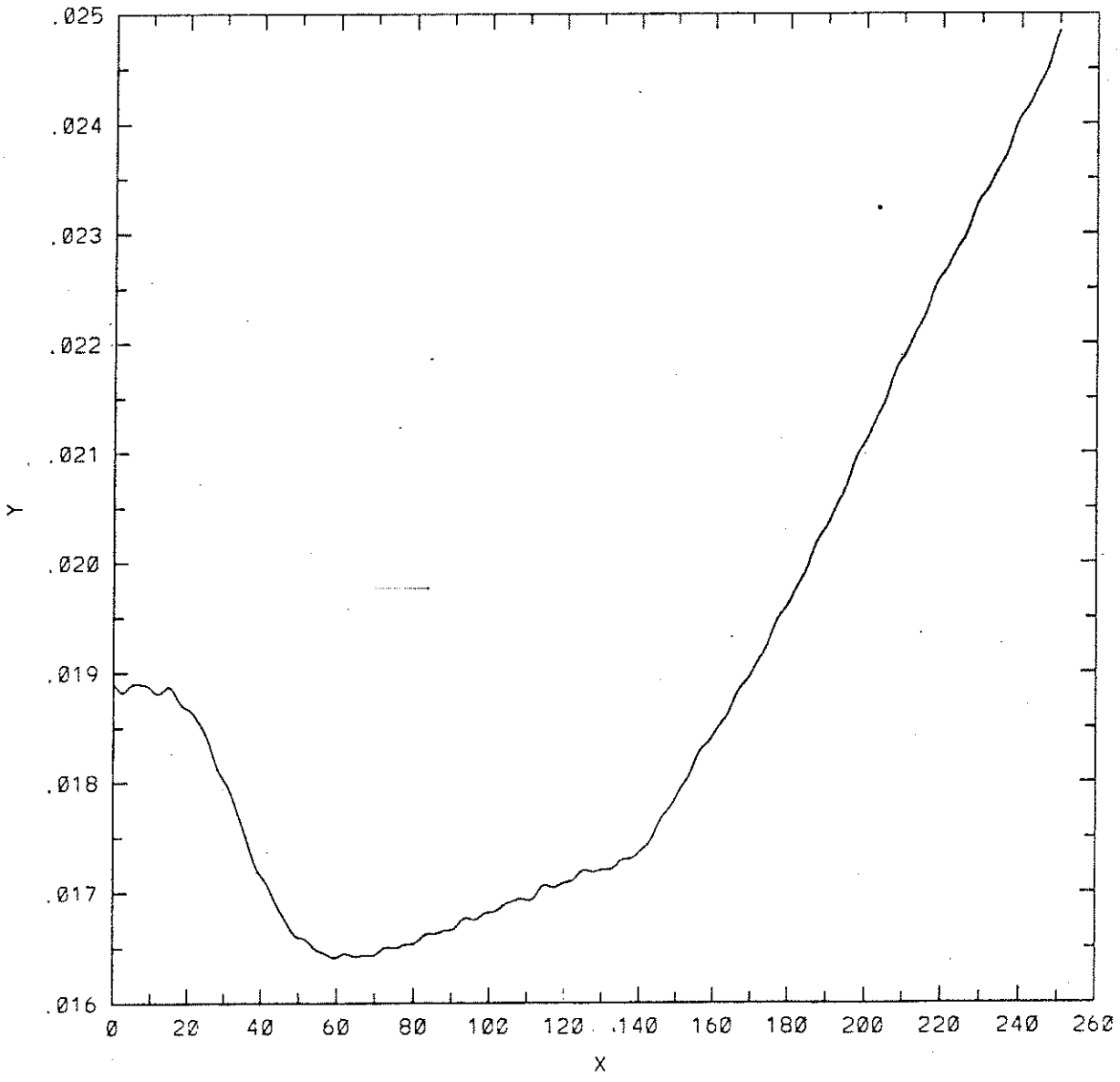

Figure 12. L^2-norm of v vs t, for $c = .438$, $\epsilon = .001$.

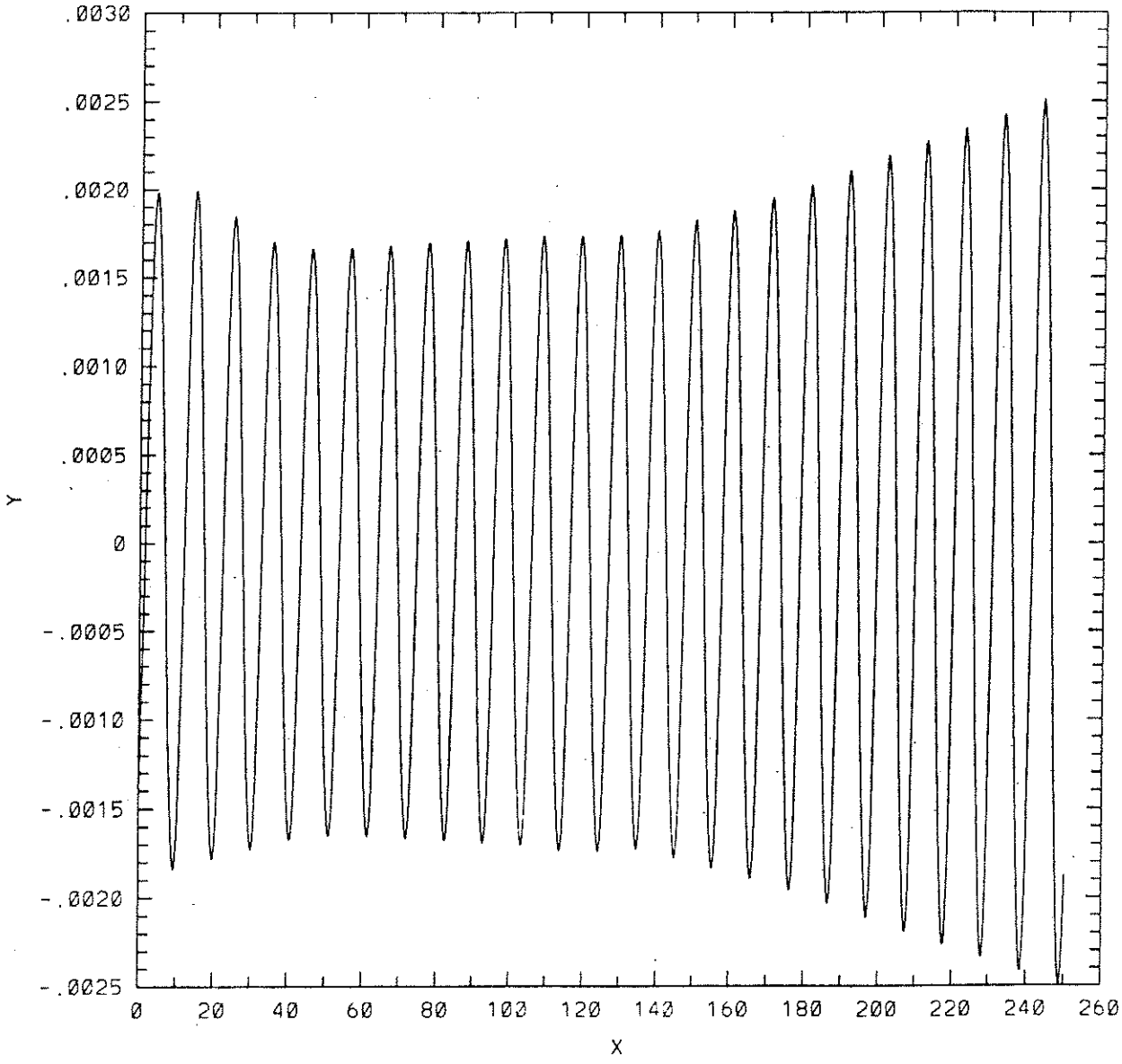

Figure 13. $v(\xi_0, t)$ vs t, for $c = .438$, $\epsilon = .001$, $\xi_0 = -16$.

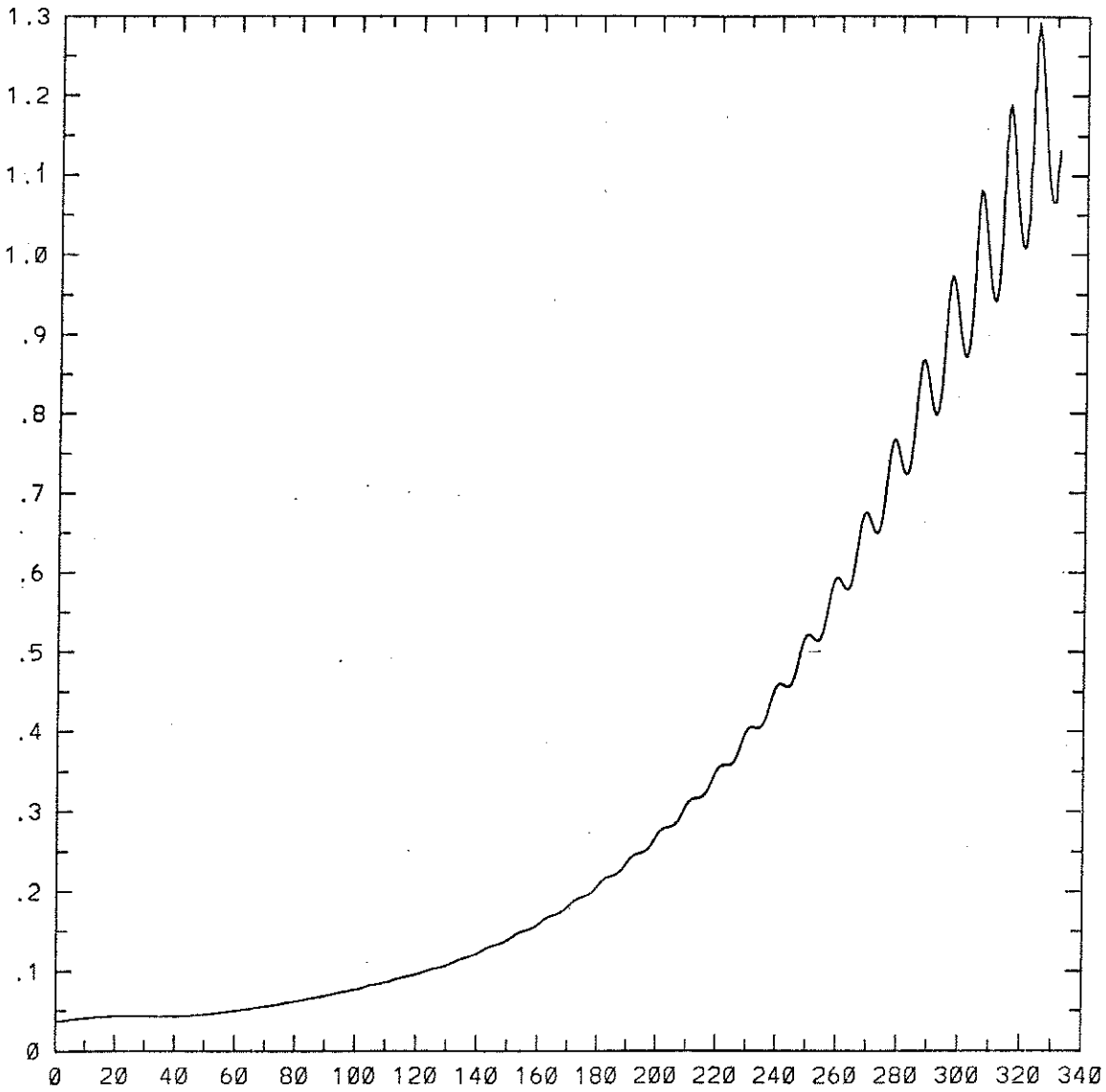

Figure 14. L^2 norm of $v(\cdot, t)$ vs t, for $c = .47$, $\epsilon = .002$.

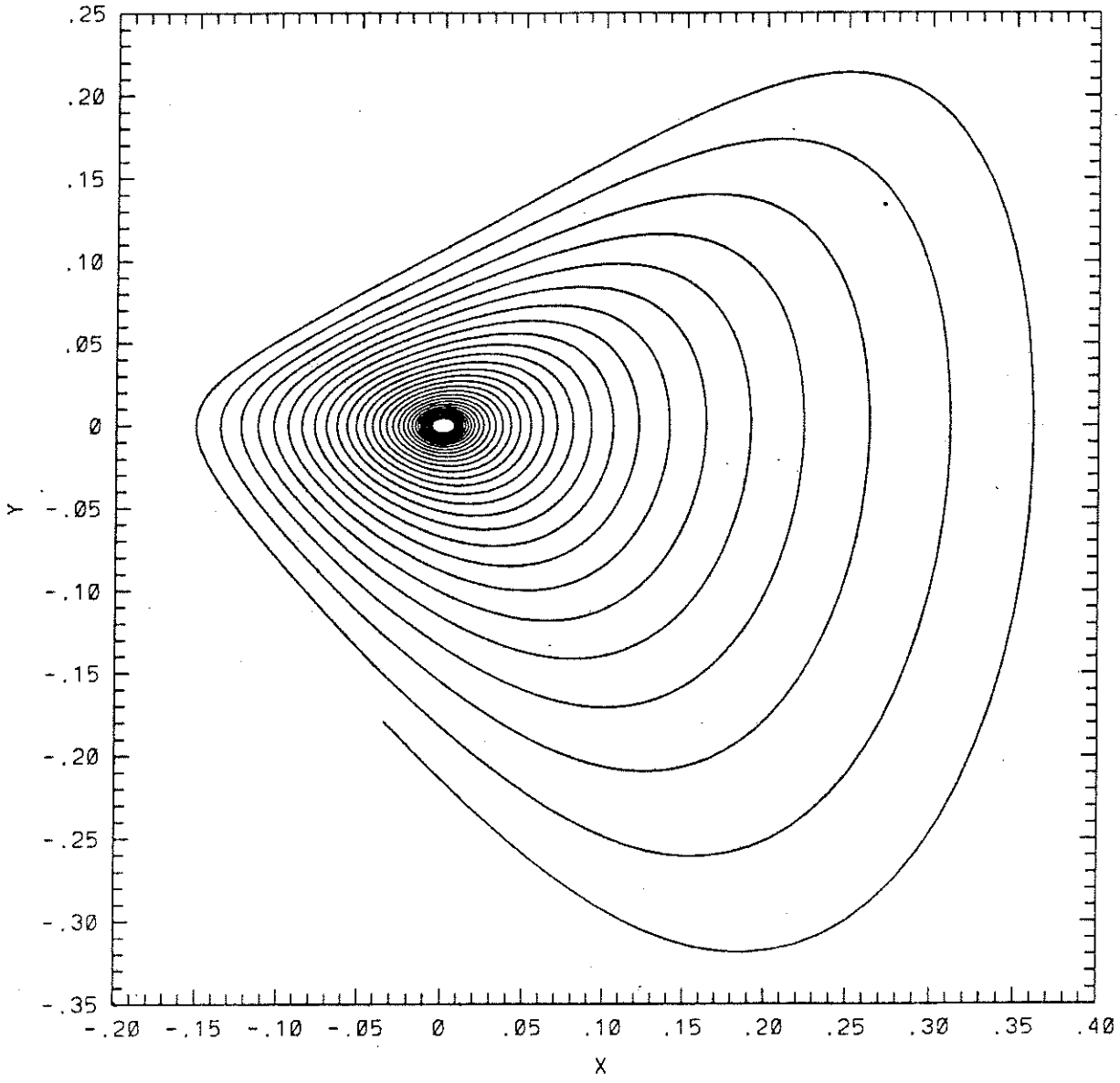

Figure 15. $\partial_t v(\xi_0, t)$ vs $v(\xi_0, t)$, for $c = .47$, $\epsilon = .002$.

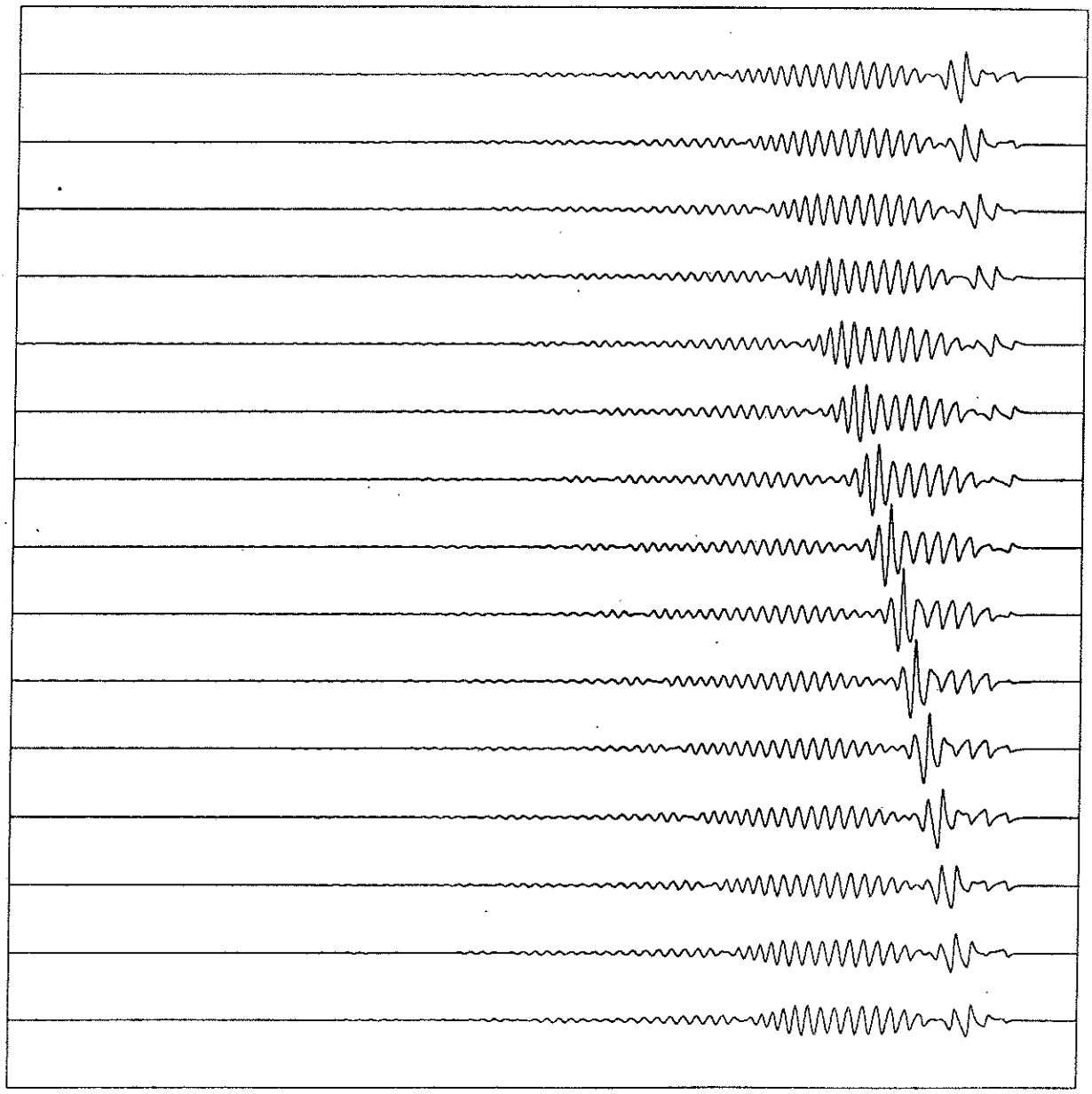

Figure 16. $v(\xi, t)$ vs ξ, for $c = .47$, $\epsilon = .002$, $t = 319, \ldots, 330$.